Journal of Hydrology 577 (2019) 123955

Contents lists available at ScienceDirect

Journal of Hydrology

journal homepage: www.elsevier.com/locate/jhydrol

Research papers

Assessing the potential impacts of climate and land use change on water fluxes and sediment transport in a loosely coupled system

Subhasis Giri*, Nazia N. Arbab, Richard G. Lathrop

Department of Ecology, Evolution, and Natural Resources, School of Environmental and Biological Sciences, Rutgers, The State University of New Jersey, New Brunswick, NJ 08901, USA

ARTICLE INFO

This manuscript was handled by G. Syme, Editor-in-Chief, with the assistance of Ji Chen, Associate Editor

Keywords:
Climate change
Land use change
Loosely Coupled Systems
Soil and Water Assessment Tool
Transition potential model
Agent-based model
Representative concentration pathways
Hydrologic cycle
Sediment load
Climate resiliency

ABSTRACT

Climate and land use change are the two primary factors that affect different components of hydrological cycle as well as sediment transport in the watershed. Quantifying potential impact of these two stressors enables decision makers to formulate better water resource management strategies to adapt to the changing environment. To that end, we have developed an integrated modeling framework employing an Agent-based approach to simulate land use conversion that then serves as input to the Soil and Water Assessment tool (SWAT) in a loosely coupled fashion. The modeling framework was tested on the Neshanic River Watershed (NRW), 142 km^2 area in central New Jersey that contains mix of urban, agricultural and forested lands. An ensemble of 10 different global climate models (GCMs) for two different greenhouse gas emission scenarios including representative concentration pathways-4.5 and 8.5 (RCP-4.5 and 8.5) were employed to model future climate from 2020 to 2045. Land use conversion for 2040 was developed based on six driving factors including distance to residential lands, agricultural lands, roads, streams, train stations, and forest using three land use transition potential models and further, the best transition potential model accompanied with some local land use restrictions.

The study evaluated various components of hydrological cycle and sediment transport for the three different scenarios one-at-a-time including climate change alone, land use change alone, and combined climate and land use change. Results indicate that the changing climate will have a larger effect on the hydrologic cycle than intensifying urban land uses in the study watershed. The climate change scenarios, either alone or in composite with land use change, predict higher streamflow (32% and 36% increase over baseline, respectively), overriding the effect of land use change which predicts a decline of 5% in streamflow. The increase in streamflow results in an increase in sediment loading, presumably due to an increase stream downcutting. Conversely, the effect of land use change (in this case the conversion of agricultural land to low density residential uses), is predicted to decrease sediment load. When modelled in composite, the effect of changing land use (in this case the conversion of erodible agricultural fields to suburban development) appears to override the adverse effect of climate change, enhancing watershed resiliency by reducing sediment load and thereby improving health of the downstream aquatic ecosystems.

1. Introduction

Climate and land use change are the two primary stressors that humanity is facing in the 21st Century (Pervez and Henebry, 2015; Teshager et al., 2016; Zhang et al., 2018); and both of them have larger implications on hydrological cycle as well as sediment transport in the watershed (Wagena et al., 2016; Panagopoulos et al., 2015; Luo et al., 2013; Boe et al., 2009). Due to increase in average global mean temperature, different components of hydrological cycle including precipitation, evaporation, transpiration, infiltration, groundwater, surface runoff, and snowmelt are going to affect seriously at both spatial and temporal scales (Immerzeel, 2008; Labat et al., 2004). Additionally, a warmer atmosphere will have greater water holding capacity leading to intensification of hydrological cycle which will pose the risk of flooding and droughts at locale to regional scale (Praskievicz and Bartlein, 2014; Wu et al., 2012a). Increased surface runoff due to climate change poses a threat of excessive land degradation in the upland areas in the watershed and significantly affects the sediment transport in the river reach systems. Similarly, changing land use will alter the energy balance within the hydrological cycle (Ma et al., 2009) affecting

* Corresponding author.
E-mail address: subhasis.giri@rutgers.edu (S. Giri).

https://doi.org/10.1016/j.jhydrol.2019.123955
Received 2 January 2019; Received in revised form 31 May 2019; Accepted 13 July 2019
Available online 18 July 2019

evapotranspiration (Mao and Cherkauer, 2009), interception (Babamaaji, 2013), infiltration (Zierl and Bugmann, 2005), surface runoff (Giri et al., 2018; Yan et al., 2013), and sediment transport (Shrestha and Wang, 2018; Bussi et al., 2016) resulting a profound impact on water quality and water supply (Giri et al., 2018; Cho et al., 2009; Kundzewicz et al., 2007). Elevating the level of sediment in the river reach systems has a negative impact towards environmental sustainability including global biodiversity and ecosystems function (IPCC, 2014).

Future climate and land use change has profound implications for the state of New Jersey as it faces severe flooding due to extreme events (USEPA, 2016) that is further exacerbated by the highest percentage of urban land cover in the U.S. (Lathrop et al., 2016). The average annual temperature in the State has increased by 2°F since 1900 whereas the average winter temperature has increased by 4°F since 1970 (Frumhoff et al., 2007; USEPA, 1997). The average annual precipitation in the State has increased by 5 to 10 percent while the major extreme precipitation events have increased 70 percent in the Northeast U.S. (USEPA, 2016; NCSL, 2008). Additionally, New Jersey being the most densely populated state provides an excellent case study of the multiple effects of intensifying urban land uses.

Considering different stressors including climate and land use change on different components of hydrological cycle and sediment transport on watershed scale requires a holistic and multidisciplinary approach to better understand the underlying cause and effect as well as sustainable adaptation strategies to mitigate the undesirable effects. Resiliency is known as capacity to adjust or develop adaptation strategies of a system to address external undesirable environmental changes (Nelson et al., 2007; Folke, 2006). Better understanding of how the changes in land use and climate will impact the hydrological cycle, and especially sediment transport, will enable more informed watershed adaptation strategies to help make communities more resilient to climate change. To that end, model simulation is proven to be an effective tool (Woznicki et al., 2016; Giri et al., 2015). A variety of models have been developed to assess the impact of climate and land use change on watershed scale, however, Soil and Water Assessment Tool (SWAT) has seen widespread application due to its process based structure, ability to model hydrology, plant growth related process, incorporate different urban and agricultural management practices, representation of land use and meteorological parameters essential from water balance prospective (Zhang et al., 2018; Giri et al., 2016a; Ficklin and Barnhart, 2014; Giri et al., 2014; Mutenyo et al., 2013).

SWAT model has not only been used to assess the effect of climate change on watershed hydrology and water quality (Shrestha and Wang, 2018; Yang et al., 2018; Reshmidevi et al., 2017; Woznicki et al., 2016;Cousino et al., 2015; Ficklin and Barnhart, 2014; Chien et al., 2013; Wu et al., 2012a), but also employed to evaluate the combined effect of land use and climate change on hydrology and water quality (Ahiablame et al., 2017; Bussi et al., 2016; Chen et al., 2017; Gabriel et al., 2016; Ma et al., 2009; Mehdi et al., 2015; Molina-Navarro et al., 2018; Neupane and Kumar, 2015; Paul et al., 2017; Pervez and Henebry, 2015; Setyorini et al., 2017; Teshager et al., 2016; Zhang et al., 2018) on watershed scale throughout the globe. In evaluating the implications of the combined effect of future land use and climate change, authors have generally projected future land use based on either hypothetical scenarios (Molina-Navarro et al., 2018; Zhang et al., 2018; Chen et al., 2017; Neupane and Kumar, 2015; Teshager et al., 2016; Mehdi et al., 2015) or using global/national scale models (Ahiablame et al., 2017; Gabriel et al., 2016; Pervez and Henebry, 2015). Hypothetical land use projection does not match with the real land use change in the ground while global/national scale models lack a nuanced consideration of local regulations or future land development plans in a region.

Most of the prior research on modeling the combined effect of land use and climate change on hydrology has focused on land development scenarios related to agricultural land conversion (i.e. conversion of other land uses to agricultural land or between various agricultural land practices). However, there is a great need to evaluate the combined effects in urbanizing regions as well to formulate water resource management strategies adapted to a changing environment. To that end, we have developed an integrated modeling framework in a coupled natural and human system where the natural system is modelled using SWAT and the urban land use conversion. To overcome the aforementioned drawbacks for land use projection, we have been exploring land use change models driven by socio-economical, regulatory as well as neighboring land use factors using both Agent-based and Transition potential modeling. The specific objectives of this study were to i) evaluate the potential impact of climate change in the near future on different components of hydrological cycle as well as sediment load on a field and watershed scale; and ii) estimate the effect of land use change only as well as combined climate and land use change on different water fluxes and sediment load in a Central New Jersey Watershed.

2. Materials and methods

2.1. Study area

The study area (Neshanic River Watershed or NRW) is located in Central New Jersey between U.S's largest and 6th largest cities (New York and Philadelphia, respectively) experiencing the effect of both climate and land use change (Fig. 1). It is a headwater to Raritan Basin. The NRW has been declared as impaired for aquatic life due to non-point source pollution such as total suspended solids and other pollutants (NJDEP, 2011). Apart from degraded water quality issues, NRW has been influenced by water quantity fluctuation especially during the low flow condition. The 142 km^2 watershed is evenly divided between agricultural, urban and forest land (32 versus 30 versus 29%, respectively) with smaller component of wetlands (8%), barren lands and water. The land use map of the NRW can be found in the Supplementary material (Fig. S1). The elevation in the watershed ranges from 20 m to 208 m above the mean sea level (Fig. 1). A recent study conducted by Giri et al. (2016b) indicates an increase in urbanized land use is expected in the watershed in the coming years.

The watershed is located in the Piedmont physiographic region and it is underlain by slightly folded and faulted sedimentary and igneous rocks. A humid climate is observed in the watershed having hot and humid during summer (average temperature of 27 to 30 °C) while cold in winter (average low temperature of −7 to −5°C). The mean annual precipitation is 1,292 mm according to National Climatic Data Center, with precipitation occurring 120 days per year. During the summer, thunderstorms are responsible for a majority of the precipitation in the watershed. The average annual winter snowfall in the watershed ranges from 120 to 770 mm. Well drained silty soils are found in the watershed where major crops including hay, soybean, pasture, winter wheat, and corn are grown. Minor crops include oat, barely, sunflower, sorghum, and rye.

2.2. Conceptual framework of loosely coupled systems

This climate and land use change study was conducted in a loosely coupled system (LCS) (Fig. 2). The LCS had two intra-systems and one inter-system interaction. The Land Use Prediction modeling component focusses on the ongoing land management and land use conversion process (i.e., conversion of agricultural and forest into residential land). The Hydrologic modeling component focused on the different components of hydrologic cycle including surface runoff, streamflow, water yield, groundwater recharge, lateral flow, evapotranspiration, soil water, and percolation as well as sedimentation. These hydrologic processes are dependent on the properties of topography, soil, land use/land cover, and management. Urbanization and the resulting increase in impervious surface affects different water balance components as

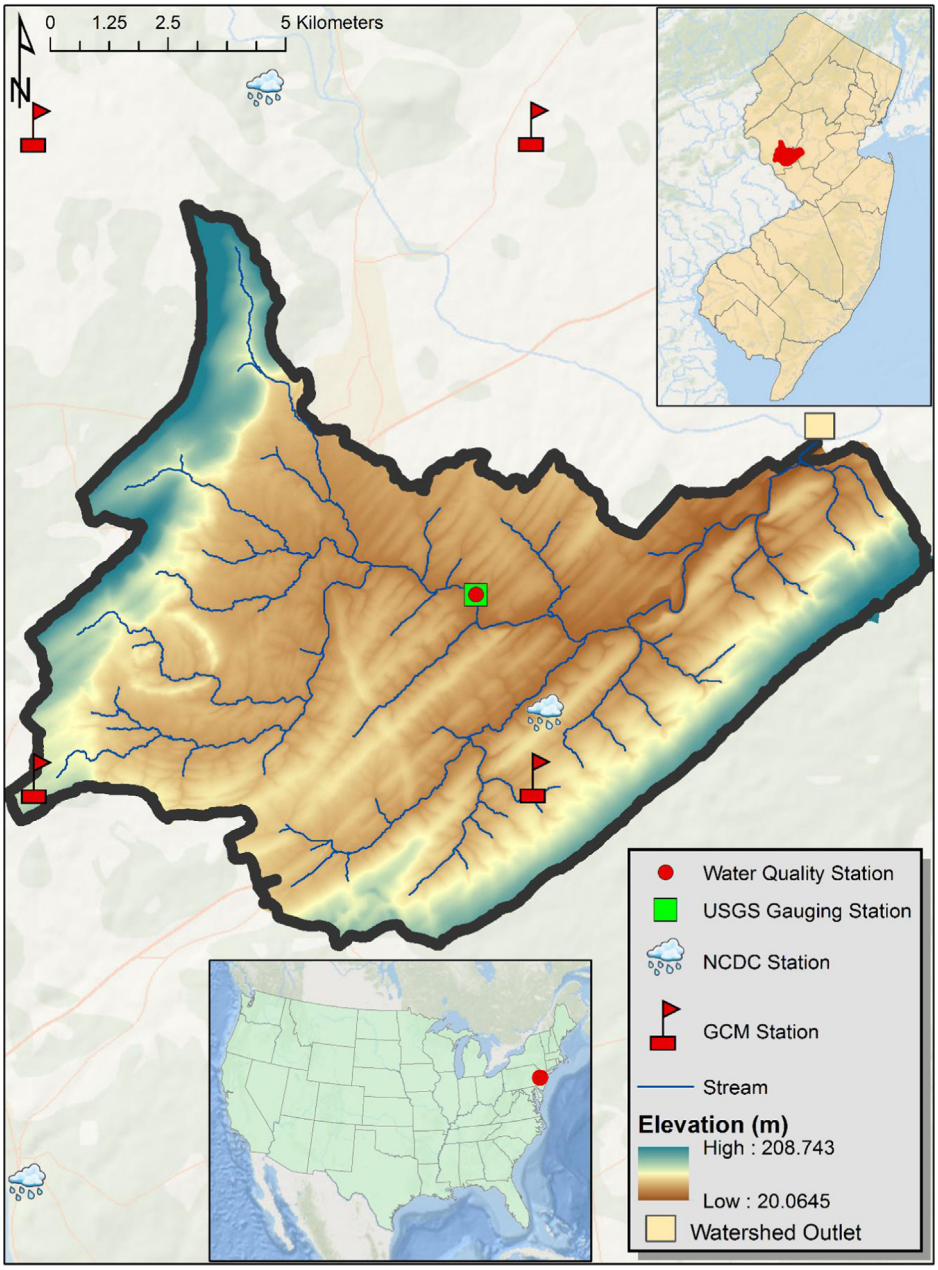

Fig. 1. Location of Neshanic River Watershed with respect to United States (bottom) and New Jersey (top right) and the watershed at the center.

well as sediment transport potentially acerbating flooding/drought and decreased downstream water quality. Climate change potentially magnifies the coupling between these two systems leading to higher storm runoff, increased watershed flashiness (rise and fall of streamflow quickly during storm events) and sediment erosion and transport.

2.3. Loosely coupled modeling framework

The loosely coupled modeling framework consisted of three strands: 1) Hydrologic modeling framework, 2) Land use prediction framework, and 3) Data analysis framework (Fig. 3).

2.3.1. Hydrologic modeling framework

2.3.1.1. Model description. The SWAT model was used to predict the different components of the hydrological cycle as well as sediment transport in the NRW. SWAT is a semi-distributed, physically based watershed scale model developed by U.S. Department of Agriculture (USDA) (Arnold et al., 1998; Gassman et al., 2007; Neitsch et al., 2011). Different primary components of the SWAT model are hydrology, soil, plant growth, weather, nutrients, pesticides, and land management practices. The hydrologic component of SWAT is divided into two parts: i) land phase hydrologic cycle and ii) routing phase hydrologic cycle. The hydrologic modeling framework consisted of three different spatial scales including hydrologic response units (HRUs), subbasin, and watershed scale. HRUs are the unique combinations of soil, land use, slope, and management within each subbasin (Arbab et al., 2019). A combination of different HRUs forms subbasins and the summation of subbasins forms a watershed. All the required inner algorithms of SWAT for this study are provided in the model description section of the Supplementary Material.

2.3.1.2. Model input data. The required inputs for SWAT model are physiographic data, streamflow, sediment concentration, and management operations. The topography of the watershed was

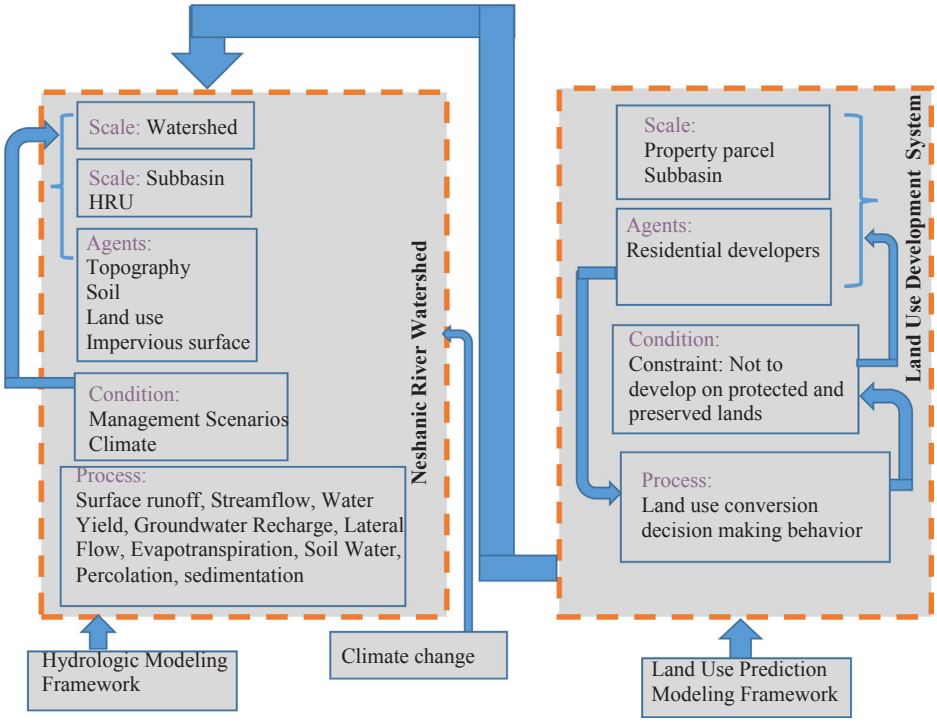

Fig. 2. Schematic of Loosely Coupled Systems components in this climate and land use change study in the Neshanic River Watershed.

presented by fine scale digital elevation model (3 m × 3 m) (NJDEP, 2018). The land use was represented by 2012-NJDEP land use (30 m × 30 m) data (NJDEP, 2012). The NJDEP land use was classified into six broader categories including urban, agricultural land, forest, wetlands, water, and barren lands. In order to represent different crop lands within the agricultural lands in the watershed, 2017 Crop Data Layer (30 m × 30 m) from U.S. Department of Agriculture National Agricultural Statistics Service was combined with 2012-NJDEP land use data in ArcGIS environment (NASS, 2017). The Soil Survey Geographic Database (SSURGO) soil data from USDA Natural Resources Conservation Services (NRCS) was obtained to represent the soil characteristic in the watershed. The meteorological data such as daily precipitation, minimum and maximum daily temperature were obtained from three National Climatic Data Center stations (Fig. 1) from 1990 to 2015.

The remaining meteorological data including solar radiation, relative humidity, and wind speed was generated from SWAT weather generator program. To accurately evaluate the fate and transport of the streamflow and sediment, different management operations including date and types of tillage, amount of fertilization, planting and harvesting date of hay, winter wheat, pasture, corn, soybean, oats, and rye were prepared by interviewing local farmers and NRCS personnel.

Urban lands were represented in SWAT model based on the percent impervious cover. The pervious part of the urban land was modelled as lawn and the management operations for the lawn such as mowing and fertilization were prepared after interviewing landscape professionals and local residents in the watershed. In this study, SWAT 2012.10_3.18 was used for the modeling purpose and the SWAT model divided the study area into 115 subbasins and 9117 HRUs. The HRUs within subbasin were created using the threshold of 1%:10%:10% for land use, soil, and slope, respectively. Using these thresholds, land use area less than 1% within the subbasin were eliminated while soil class less than 10% within each land use were eliminated, and slope class that did not have at least 10% within soil were removed during formation of HRUs.

2.3.1.3. Climate change scenarios. Policymakers generally focus on events occurring in the near term compared to the events in the distant future as they look at the distant future events in more abstract terms (Weber, 2006). Consequently, we selected the climate change data in the near term (2020 to 2045) rather than for the end of the century. Two greenhouse gas emission scenarios known as representative concentration pathways (RCP-4.5 and RCP-8.5) were selected. RCP-4.5 represents the mid range emission/moderate reduction scenario while RCP-8.5 depicts high emission scenario/business as usual (IPCC, 2014). The climate change scenarios under RCP-4.5 and 8.5 were projected based on the SWAT simulation period 2021 to 2045 while for the base period was from 1991 to 2015.

Ten different Global Circulation Models(GCMs) from Coupled Model Intercomparison Projects (CMIP5) including BCC-CSM1-1, CANESM2, CCSM4, CSIRO-MK3-6-0, GFDL-ESM2G, INMCM4, IPSL-CM5A-LR, MIROC-ESM, MPI-ESM-LR, and NORESM1-M were selected for this study as these GCMs are appropriate for North America (Sunde et al., 2018; Shrestha and Wang, 2018; Cousino et al., 2015;Culbertson et al., 2016). The detail about the models such as modeling center can be found in the Table S1 of the Supplementary Material. The daily precipitation and minimum and maximum temperature based on each GCM were downloaded for historical (1990–2015) as well as future (2020–2045) for the study area from the United States Bureau of Reclamation (USBR). The total number of scenarios with combination of two types of RCP, 10 GCMs, and two time periods was 40 (2 × 10 × 2). This climate data used a statistical downscaling method known as daily bias correction and constructed analogs (BCCA) to correct the systematic errors in GCMs and were downscaled to a spatial resolution of 1/8°. More information regarding climate data and downscaling method used in this study can be found from Brekke et al.(2013). The remaining meteorological data including solar radiation, relative humidity, and wind speed were estimated using SWAT weather generator.

Elevated CO_2 level increases plant productivity and decreases plant water requirement due to partial stomatal closing which might reduce the evapotranspiration (Cho et al., 2009; Barton et al., 2012). However, the response of evapotranspiration to elevated CO_2 under high end scenario is questioned and it is still under debate in the scientific community (Molina-Navarro et al., 2018; Karlsson et al., 2015; Peng et al., 2014). In this study, we have not changed the CO_2 concentration

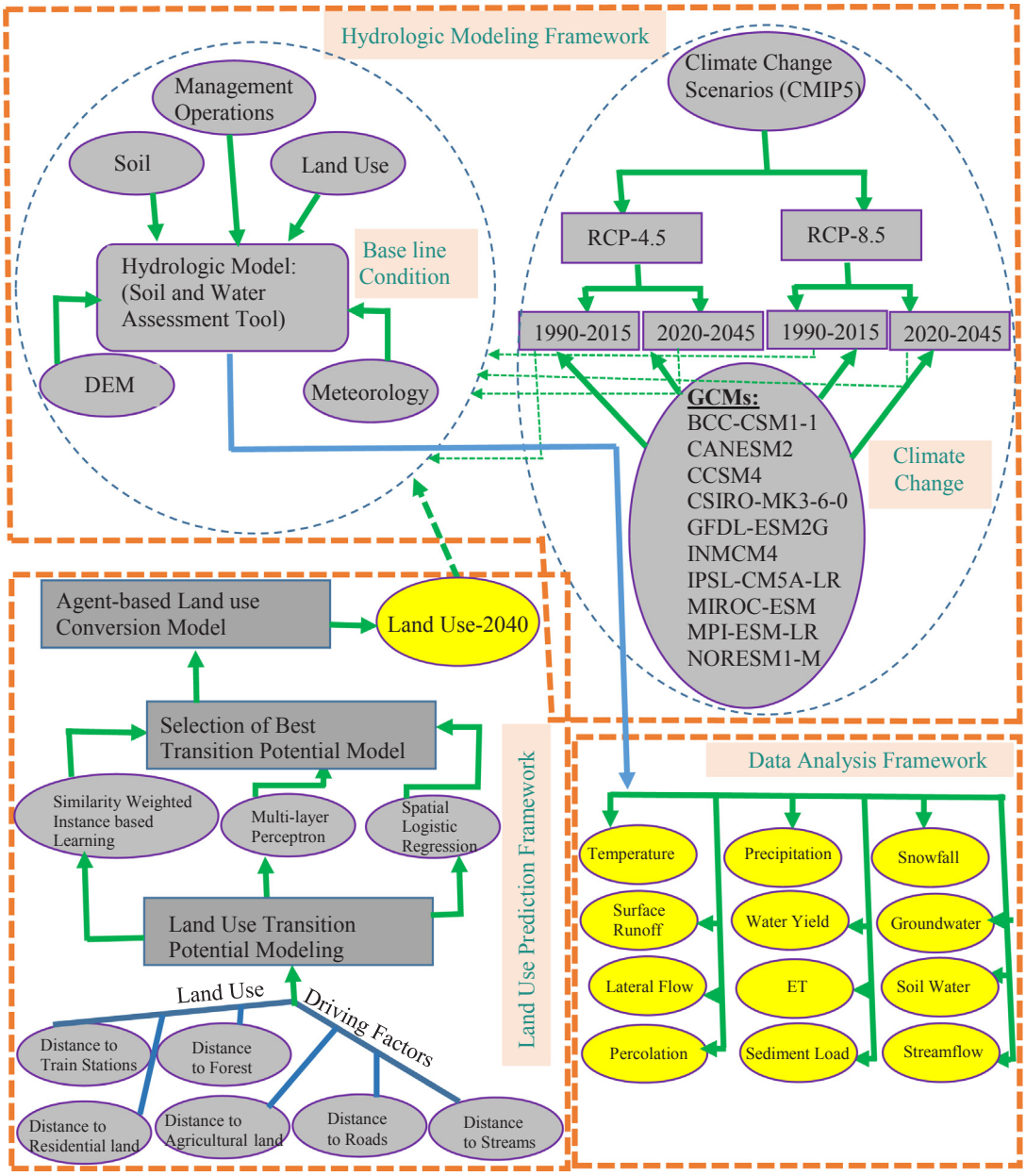

Fig. 3. Schematic of loosely coupled modeling framework in the climate and land use study in the Neshanic River Watershed.

of the various RCP scenarios due to the uncertainty involved.

All climate data were incorporated in the calibrated SWAT model one-at-a-time and ran separately on a monthly time scale for two different time periods: i) 1990–2015 (historical) and ii) 2020–2045 (future). First, the streamflow generated by each GCM for 1990–2015 time period at USGS gauging station 01,398,000 (Fig. 1) was compared on a monthly basis to the observed streamflow using both visually and paired two sample *t*-test. Additionally, monthly streamflow from 10 GCMs were averaged to estimate the ensemble mean and the ensemble mean of monthly streamflow was compared with the observed streamflow by both visually and paired two sample *t*-test. The ensemble mean approach was adopted to reduce individual biasness of GCM which would ultimately reduce the uncertainty in the climate change study (Sunde et al., 2018; Culbertson et al., 2016; Wagena et al., 2016).

2.3.1.4. Sensitivity analysis and calibration. Sensitivity analysis is performed to determine the most influential parameters in watershed modeling where modeler uses most sensitive parameters during model calibration process. The most sensitive parameters for streamflow and sediment were conducted by past studies in the same watershed including Giri et al.(2018), Giri et al.(2016a), and Qiu and Wang (2014). A total of 16 streamflow and five sediment sensitive parameters were collected from the previous studies. Furthermore, these parameters were used in the SWAT-CUP (Abbaspour 2012; Abbaspour et al., 2007) along with the Sequential Uncertainty Fitting (SUFI-2) algorithm (Abbaspour et al., 2004) for calibration and validation.

The streamflow and sediment were calibrated and validated using the objective function of Nash-Sutcliffe efficiency (NSE) in SWAT-CUP. Further, SWAT model performance was evaluated using three model evaluation parameters including NSE, Percent bias (PBIAS), and Root mean square error (RMSE)-observations standard ratio (RSR). The detail about these model evaluation parameters can be found in the Supplementary Material. Two years (2002–2003) of warm up period was used to initialize model parameters for ideal simulation. The SWAT model was calibrated using a monthly time step between 2004 and 2009 while it was validated for 2010–2014.

The monthly streamflow data used for calibration and validation were collected from U.S. Geological Survey (USGS) for the USGS gaging station 01,398,000 (Fig. 1). The daily sediment concentration was collected from USGS for the same USGS gauging station 01398000. In order to convert the daily sediment concentration to monthly loads, the USGS Load Estimator (LOADEST) was used (Wagena and Easton, 2018; Giri et al., 2012; Love and Nejadhashemi, 2011). LOADEST is developed based on FORTRAN program by USGS to help researchers and scientists to fill up the sparse water quality data for different analysis by estimating the water quality load for the user specified time period (Runkel et al., 2004). The USGS gauging station 01,398,000 is capturing streamflow from half of the watershed area. Therefore, the optimized parameters developed during calibration and validation process can be applied to the downstream watershed area due to having similar physiographic characteristics (Tables S2 and S3 Supplementary Material). Furthermore, this approach was successfully tested by Qiu and Wang (2014) in the same watershed using the same USGS gaging station for watershed restoration study using SWAT model. Other studies around the globe (Sunde et al., 2018; Molina-Navarro et al., 2018; Luo et al., 2013; Jha et al., 2007) also used similar techniques in calibrating the SWAT model for climate change study where they optimized calibration parameters using gaging stations located at center to three-fourth of the watershed area depending on the availability of observed streamflow.

2.3.2. Land use prediction framework

The human system was formulated in a land use prediction modeling framework which consists of steps for (i) specifying the driving factors of land use change, (ii) simulating the sub-models of land use change predictions, (iii) calibrating the model with best Receiver Operator Characteristic (ROC) value in agent-based model (ABM) with respect to the drivers from the land use system and, finally (iv) simulating the ABM (Fig. 3). The spatial land use output from the ABM is linked (loosely coupled) to watershed system to estimate the impact of land use change due to human decision making on water systems.

2.3.2.1. Model description. A transition potential map shows the relative likelihood of transition of a particular pixel of particular land use land cover (LULC) class which simulated based on the transition of LULC in the calibration period (Camacho Olmedo et al., 2013; Mas et al., 2014; Mozumder et al., 2016). The choice of the land use transition LULC models is dependent upon the tradeoffs of each model and the peculiarities of the study area.

This study compares three land use change modeling techniques, Multi-Layer Perceptron (MLP), Spatial Logistic Regression (SLR), and Similarity Weighted Instance-based Learning (SimWeight), to estimate the future land use transitions. The MLP Neural Network technique is a machine learning approach in simulating complex linear and non-linear relationship between the various driving variables and the land use changes (Bhatti et al., 2015; Oñate-valdivieso and Bosque, 2010; Pijanowski et al., 2002; Thapa and Murayama, 2012). The SimWeight is another machine learning approach and requires less computationally intensive simulation than the MLP (Sangermano et al., 2010a,b). Spatial logistic regression analysis is a commonly used approach to estimate the influence of driving factors on spatial land use trends. Logistic regression incorporates binary dependent variables as a presence or absence of occurrence and suitability for discrete, categorical, or continuous explanatory variables (Atkinson and Massari, 1998; Lee, 2005).

All these models were implemented in TerrSet software developed by Clark labs (2018). Driver variables used in all three models were: proximity to roads, streams and train stations and proximity to agriculture, urban and forested areas. After each model was calibrated for NRW study area for an initial period 1986–2012, the model was used to predict land use change for 2040. The transitions of one land cover state to another was identified through previously mentioned three modeling techniques. We compared each model's relative ROC statistics. The ROC is suggested as a reliable approach for model validation by several studies (Pontius and Schneider, 2001; Dendoncker et al., 2007; Arsanjani et al., 2013). The ROC assess the validity of model that predicts the location of conversion by comparing the actual change between 1986 and 2012 in a Boolean map and the suitability (fitted) change between 1986 and 2012 (Swets, 1986; Pontius and Schneider, 2000; Verburg et al., 2002; Pijanowski et al., 2009; Tayyebi et al., 2010; Clark Labs, 2018). The ROC varies between 0 and 1. Within the ROC range, 1 shows a perfect fit and 0.5 shows a random fit. The larger ROC values show the better association between explanatory variables and dependent variable (Clark Labs, 2018).

2.3.2.1.1. Similarity weighted Instance-based learning. SimWeight is an instant-based machine learning land use transition potential model that is derived from the logic of the K-Nearest Neighbor procedure (Fix and Hodges, 1951). The model was formulated by calculation of weighted distances in land use variable (driving factors) space to actual land use change instances based on two time period for the land use classes. For each pixel in the raster map, the class membership is calculated as defined by Sangermano et al. (2010a,b):

$$Membership_{change} = \frac{\sum_{i=1}^{c} 1.0 - \frac{1}{1+e^{1/d_i}}}{V} \; (c \leqslant V) \quad (1)$$

where V is the number of closest land pixels (change + persistence) of a pixel, c is the number of change pixels within the m nearest neighbors and d is the distance to a change instance i. A large class membership for the change class would mean that a pixel has environmental conditions similar to those that have already changed, and therefore it can be considered to have a high transition potential.

Variable importance weight is determined by comparing the standard deviation of the variable inside the land use areas that have changed, to the standard deviation of the variable for the study area as in defined by Sangermano et al. (2010a,b) in Eq. (2):

$$\text{Relevance Weight} = 1 - (SD \text{ in change/SD in study area}) \quad (2)$$

If the variable is influencing the change, then the standard deviation (SD) of the variable inside the raster cells that changed would be smaller than for the study region as a whole, therefore having a large weight. Using this method, weights are calculated by SimWeight model for each variable (Table 1). Then, the standardized variables are multiplied by the weight. Thus changes the scale of variable in a way proportional to the importance of the variable to discriminate change. A threshold of 0.01 was set in SimWeight model to remove variables that have a very low weight.

2.3.2.1.2. Multi-Layer Perceptron (MLP). Neural networks in MLP are non-linear. MLP use complex mathematical function that converts input data such as land use raster map to a desired output, a land cover classification (Clark labs, 2018). A typical MLP network contains one input layer, one output layer and one or more hidden layers. Each layer contains nodes (or neurons) and is connected by lines indicating unequal connecting weights. The hidden layer nodes are critical in use of interaction effects to the functioning of MLP. Research indicates that a 3-layered MLP network can approximate any polynomial function, and is capable of solving very complex regression and classification problems (Clark labs, 2018). To determine MLP's prediction accuracy, the expected accuracy rate is assigned as a

Table 1
Independent variables and their relevance weights for the study area.

Variable	Relevance Weight
Distance to urban areas	0.14
Distance to agricultural areas	0.99
Distance to forest	0.15
Distance to streams	0.12
Distance to train stations	0.17
Distance to roads	0.29

function of the number of transitions being modeled along with the number of persistence classes as follows (Clark labs, 2018):

$$E(A) = 1/(T + P) \quad (3)$$

where E(A) = expected accuracy, T = the number of transitions in the submodel,

P = the number of persistence classes = the number of "from" classes in the sub-model.

A measure of model skill (prediction accuracy) is then expressed as:

$$Q = (A - E(A))/(1 - E(A)) \quad (4)$$

where A = measured accuracy, E(A) = expected accuracy.

This measure varies from −1 to + 1 with a skill of 0 indicating random chance.

The MLP algorithm was used with Natural Log transformation for distance-based variables and the Evidence Likelihood method was used to transform categorical factors. Selection of the distance based variables was based upon the fact that these variables are representatives of important parameters for physical, biological and socio-economic environments and have been found important for LULC change modeling studies (Guan et al., 2011; Sang et al., 2011; Arsanjani et al., 2013; Sakieh et al., 2015; Nasiri et al., 2018). MLP model was developed and transition potential maps were generated by quantifying the relative importance of each variable to the land use change process. Transition potential maps from MLP represent the potential of a given category for transformation to another LULC type. The LULC change process was predicted up to the year 2040.

2.3.2.1.3. Spatial logistic regression. To estimate land use conversion probabilities, driving factors of land use conversion were estimated to examine the probability of land use conversion during the period 1986–2012 as per suggested in Arbab et al. (2016). To examine the change in spatial residential land use patterns, a spatial logistic regression analysis was developed to estimate the influence of driving factors on spatial land use trends. Logistic regression offers the functionality to incorporate binary dependent variables as a presence or absence of occurrence and suitability for discrete, categorical, or continuous explanatory variables (Atkinson and Massari, 1998; Lee, 2005).

The empirically estimated relationship between the conversions of residential development and the driving factors can be expressed as the following logistic functional form:

$$P(Y = 1|x) = \frac{exp^{(\sum \beta X)}}{1 + exp^{(\sum \beta X)}} \quad (5)$$

where P(Y = 1|X) is the predicted probability value of the binary or dichotomous dependent variable Y, where Y = 1 means if a cell in raster map changes from a non-residential land use in 1986 to residential land use in 2012 and Y = 0, otherwise. This logistic function has linear probability in a set of parameters by having the range of probability between zero and one. The following linear logit transformation on both sides of Eq. (5) was used to estimate the β coefficients (Menard, 1995):

$$Y = logit(p) = ln\left(\frac{p_k}{(1 - p_k)}\right) = \beta_0 + \beta_1 x_{1k} + \beta_2 x_{2k} + \beta_3 x_{3k} + \beta_4 x_{4k} + \beta_5 x_{5k} + \beta_6 x_{6k} \quad (6)$$

Y is the probability that the dependent variable (Y) is 1, p_k is the predicted probability of the k^{th} pixel of agricultural or forest land use conversion to residential land, $\beta_0$is the intercept, and β_1, β_2, β_3, β_4, β_5, and$\beta_6$are coefficients for distance to the existing agriculture (x_1), distance to the existing forests (x_2), distance to the existing residential areas (x_3), distance to streams (x_4), distance to major highways (x_5), and distance to trains stations (x_6), respectively. These coefficients measure the influence of each independent variable on the variations in probability of land use conversion from non-residential land use to residential land use (Y).

2.3.2.1.4. Validation & Agent-based model. To examine more carefully how we did with the specific task of predicting change to land use conversion, we used a three-way cross tabulation between the later land cover map, the prediction map and the map of reality. To evaluate this, we calculated the ROC statistic (also known as the Area under the Receiver Operating Characteristic Curve - or AUC). This measure was used to determine how well a continuous surface predicted the locations given the distribution of a Boolean variable.

We selected the model parameters to be used for ABM empirical parametrization upon ROC values. This model was designed to simulate land use decisions of agricultural and forest land owners to convert undeveloped land to residential land and implemented in python programming language. The agents' conversion decisions varied with the spatial distances from each neighboring land use over a period of 10 iterations (to roughly approximate a 10 year time period), where each iteration was assumed to be a conversion event possibility. By modifying an approach from Benenson and Torrens (2004), each parcel agent's probability of conversion from developable state m to residential state r in each iteration was modeled as:

$$\Pr ob_i(S_m \rightarrow S_t) = S(N(i)) \quad (7)$$

where N (i) represented parcel agent i's neighbors and S represented state of parcel i. The model used a Monte Carlo process (Hagerstrand, 1965; Wu, 2002) for generating a stochastic ABM model. To account uncertainty, a probability function was implemented to condition the residential conversions utilizing a random number generator (Batty, 2012; Arbab, 2014). For undeveloped parcels, the conversion decision was based upon a comparison between the random number generated and the probability value for each parcel. The random number generator rand (φi) had a random distribution that was uniform between 0 and 1. The parcel agents adopted the following rule of land use conversion in each iteration.

$$\text{if rand}(\varphi_i) < P_{it} \text{ then } A_{it} + 1 = r$$

where r represented the land use class of residential development. P was the probability of conversion to residential development for each parcel i, A was the conversion event and t was iteration. Agents first assessed the parcel by comparing the probability with a random number. If the value of probability was higher than the random number, the agent converted the parcel into a residentially developed parcel. If not, then the parcel remained in its current non-developed state. The model with better ROC values was used to calibrate projections of residential land use conversions in ABM model.

The ABM modelling landscape consisted of property parcels, a decision making unit for residential developers. The model assumed a market where developable properties were available for residential developers and selection and conversion of property parcels were inherently based upon the proximity based criteria of neighboring features. The ABM model did not allow developers to build on protected and preserved forest or agricultural lands (Fig. 2). The parameter value of driving factors determined the emergent output of the ABM model. For example, positive sign of a parameter showed that high value of proximity leads to high conversion and negative parameter sign showed inverse relationship between proximity and conversion.

2.3.2.2. Model input data

2.3.2.2.1. Land use. Land use data was extracted from the NJDEP for the years 1986 and 2012 to analyze the change from 1986 to 2012. The NJDEP land use data was further categorized into six broader categories such as urban, forest, wetlands, agricultural land, water, and barren land. The raster files were created in ArcGIS 10.3.1 using Euclidian distance tool for distance to agricultural lands, distance to forest and distance to residential lands.

2.3.2.2.2. Distance to streams. The digital hydrography stream network was derived from NJDEP data.

2.3.2.2.3. Distance to highways. The data consisted of major highways including interstates, U.S. highways, state highways, and major roads. This dataset was obtained from the Census 2000. Generally, road features do not change over long periods of time, therefore, this data was found suitable for our analysis.

2.3.2.2.4. Distance to train stations. The data on transportation was extracted from New Jersey Department of Transportation (NJDOT) for creating the raster file on distance to trains stations.

2.3.3. Data analysis framework

Different SWAT model outputs including temperature, precipitation, snowfall, surface runoff, streamflow, water yield, groundwater, lateral flow, evapotranspiration, soil water, percolation, and sediment yield, and sediment load were extracted from various scenarios (base period, historical RCP-4.5, historical RCP-8.5, Future RCP-4.5, and Future RCP-8.5). These data were processed using ArcGIS environment, Matlab, R-platform, and Microsoft Excel based on the requirements for better visualization and easy understanding.

3. Results and discussion

3.1. SWAT model calibration, validation, and uncertainty analysis

Based on the previous three studies in the same watershed (Qiu and Wang, 2014; Giri et al., 2016a; Giri et al., 2018) as well as using SWAT-CUP (Abbaspour et al., 2007) and its SUFI-2 algorithm (Abbaspour et al., 2004), we found curve number, soil evaporation compensation factor, hydraulic conductivity in the main channel, maximum canopy storage, base flow alpha factor, deep aquifer percolation fraction, surface runoff lag coefficient, groundwater delay time, groundwater revap coefficient, available water capacity of the soil layer, manning's n for overland flow, manning's n for main channel, threshold depth of shallow aquifer, threshold depth for revap, snowmelt base temperature, and snowpack temperature lag factor are the most sensitive parameters for streamflow. The most sensitive parameters for sediment are exponent parameter for channel-sediment routing, linear parameter for channel-sediment routing, channel erodibility factor, channel cover factor, and universal soil loss equation support practice factor. The final values of the calibrated parameters for streamflow and sediment are presented in the Table S4 of Supplementary Material.

The model accuracy for streamflow is categorized as "very good" based on the guideline developed by Moriasi et al.(2007) due to NSE = 0.76, PBIAS = 9.52, and RSR = 0.49 for overall period (Table 2). The hydrograph between observed and simulated streamflow shows a very good agreement between the two in the watershed (Fig. 4). However, the model underestimates the peak flow slightly which may be attributed to flashiness of stormwater runoff in the watershed. A similar results of flashiness was also observed among the three previous studies in the watershed by Qiu and Wang, 2014; Giri et al., 2016a; Giri et al., 2018. This flashiness may be attributed due to inability of SWAT model to incorporate different stormwater infrastructure including detention basins, swale, ditch segments, detention basin inflows, discharge pipe, and outfalls. The model evaluation parameters for sediment suggests that SWAT model performance is "satisfactory" in predicting the sediment load in the watershed (Table 2). The time series of observed and simulated sediment load in the watershed is presented in the Supplementary Material (Fig. S2) which suggests that the overall prediction of sediment load by SWAT model agrees with observed sediment load with exception of few under predicted peaks. This trend may be due to the SWAT model's inability to capture the flashiness of the streamflow.

Table 2
SWAT model evaluation parameters for streamflow and sediment in the Neshanic River Watershed.

Constituents	Evaluation parameters	Overall period (2004 to2014)	Calibration period(2004 to 2009)	Validation period(2010 to 2014)
Streamflow	NSE	0.76	0.78	0.75
	PBIAS	9.52	13.13	4.67
	RSR	0.49	0.47	0.50
Sediment	NSE	0.61	0.63	0.57
	PBIAS	24.21	27.42	17.17
	RSR	0.62	0.61	0.65

The primary source of uncertainty in climate change studies comes from the projected climate data (Molina-Navarro et al., 2018; Trolle et al., 2015; Jensen and Veihe, 2009). Therefore, we undertook an uncertainty analysis by comparing the predicted monthly streamflow from 1990 to 2015 of individual GCM from RCP-4.5 and 8.5 emission scenarios against the observed streamflow data at USGS gauging station (Fig. 1) in the watershed. The average 26-years monthly streamflow shows reasonable agreement between observed versus individual GCM (Fig. 5). In fact, the streamflow between observed and ensemble mean depicts higher agreement. Furthermore, performance statistics including NSE, PBIAS, and RSR between observed and ensemble mean streamflow (Table S5 Supplementary material) shows satisfactory based on the guideline developed by Moriasi et al.(2007). In general, a "V" shape trend was observed for streamflow throughout the year where one end of the vertex is represented by streamflow at the month of January while the other end of the vertex shows the streamflow during the month of December. The vertex represented at streamflow during month of July. Additionally, NCDC simulated streamflow was plotted with observed and ensemble mean which depicts closer trends of streamflow with observed compared to ensemble mean (Fig. 5).

In general, individual GCMs as well as the ensemble mean of streamflow over predicts the observed streamflow, especially during summer and fall seasons. A similar trend was observed between individual GCM as well as ensemble mean versus observed streamflow for RCP-8.5 emission scenario (Fig. S3, Supplementary Material).

In order to determine the significant differences between average monthly streamflow from individual GCM as well as ensemble mean versus observed streamflow from 1990 to 2015, a paired two sample *t*-test (between individual GCM/ensemble mean versus observed streamflow) for mean was conducted in R-platform. Monthly average streamflow under RCP-4.5 emission scenario from individual GCMs except CANESM2 shows an insignificant difference with observed streamflow at least 1 percent level of significance (Table 3). Furthermore, the ensemble mean streamflow also depicts insignificant difference with observed streamflow. A similar result was also observed under RCP-8.5 emission scenario (Table S6, Supplementary Material). Due to presence of significant difference in average monthly streamflow between CANESM2 versus observed streamflow under both RCP-4.5 and 8.5 scenarios, the CANESM2 was not included while calculating the ensemble mean during RCP-4.5 and 8.5 emission scenarios from 2020 to 2045. Consequently, the results of each components in the hydrological cycle as well as sediment transport in the future scenarios (i.e, 2020 to 2045) was calculated based on ensemble mean of all the individual GCMs except CANESM2. The performance of individual GCMs except CANESM2 is more likely to perform better in the future condition compared to the CANESM2 which already performed poor during current condition (1990 to 2015) (Teutschbein and Seibert, 2012).

3.2. Land use conversion based on agent-based probabilistic and transition potential model

The land use conversion model results showed that SLR had a higher ROC value than the other two land use prediction modeling techniques (Table 4).

The parameter values were calibrated through spatial logistic regression and incorporated into agents' land use conversion decisions.

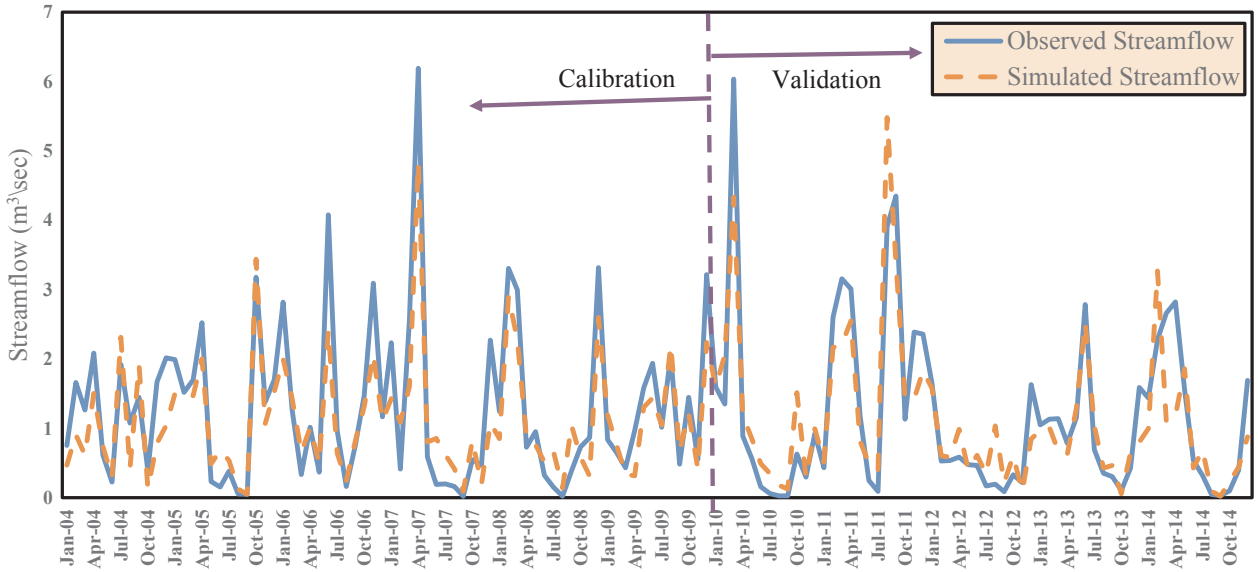

Fig. 4. Simulated and observed streamflow hydrographs at United States Geological Survey gauging station 01,398,000 in the watershed for this climate and LULC change study.

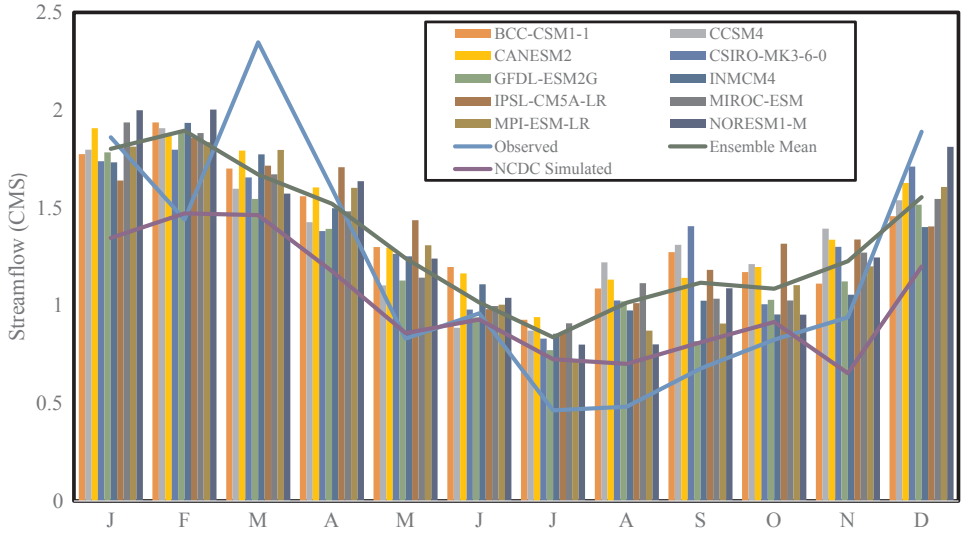

Fig. 5. Average monthly streamflow of individual GCM, observed, and ensemble mean for RCP-4.5 scenario in the Neshanic River Watershed from 1990 to 2015. The x-axis represents months starting from January to December.

Table 3
Comparison of average monthly individual GCM and ensemble mean versus observed stream flow from 1990 to 2015 under RCP-4.5 emission scenario.

GCMs	Mean 1	Mean 2	Variance 1	Variance 2	Df	t-Stat	P-value
BCC-CSM1-1	1.19	1.37	0.38	0.10	11	−1.55	0.15
CANESM2	1.19	1.42	0.38	0.11	11	−2.21	0.04***
CCSM4	1.19	1.36	0.38	0.11	11	−1.27	0.23
CSIRO-MK3-6–0	1.19	1.34	0.38	0.11	11	−1.29	0.22
GFDL-ESM2G	1.19	1.25	0.38	0.14	11	−0.5	0.63
INMCM4	1.19	1.30	0.38	0.13	11	−1	0.34
IPSL-CM5A-LR	1.19	1.37	0.38	0.10	11	−1.47	0.17
MIROC-ESM	1.19	1.33	0.38	0.13	11	−1.32	0.21
MPI-ESM-LR	1.19	1.31	0.38	0.16	11	−1.3	0.19
NORESM1-M	1.19	1.35	0.38	0.19	11	−1.57	0.15
Ensemble Mean	1.19	1.33	0.38	0.12	11	−1.30	0.21

*** indicates significant with at least 1 percent level of confidence.

Table 4
Receiver Operator Characteristic (ROC) value in each land use prediction model.

Models	ROC Value
MLP	0.277
Sim Weight	0.410
SLR	0.860

Table 5
Area of land use converted into residential land based on each model.

Model	From agricultural land (ha)	From forest (ha)	Total converted area (ha)
MLP	142.99	166.08	309.08
Sim Weight	125.86	245.76	371.63
SLR based ABM	2,785.53	890.33	3675.86

The βX function representing conversion event is calculated using the following equation:

$$\beta X = 1.288 - 0.0015*agric_{dist} + 0.0008*forest_{dist} + 0.0013*resid_{dist} + 0.0007*stream_{dist} - 0.0002*highway_{dist} - 0.00005*train_{dist} \quad (9)$$

The SLR βX function coefficients suggest that new residential conversions were not positively associated with proximity (i.e. the inverse of distance from) to existing residential lands forests or streams. Conversely, proximity to agricultural lands, highway and train stations associated with residential conversions.

Compared to MLP and SimWeight, the SLR based ABM model resulted in a significantly larger area converted to urban land (Table 5). The different outcomes between machine learning methods and regression based ABM is likely due to the difference in the underlying construction of the land conversion models; the MLP and SimWeight models are based on a grid cell geometry while the SLR ABM is based on polygonal parcels (i.e., the entire ownership parcel may convert at a single time step). While all three models displayed a preference for the conversion of agricultural land to urban land uses, the ABM converts a significantly higher amount of land overall (Table 5 and Fig. 6). The ABM is more similar to a "build-out model" where all available agricultural land (that isn't protected as preserved farmland) and forest land that isn't protected by regulation is converted. Based on the higher ROC value, as well as the larger amount of land use area predicted to convert by 2040, the ABM results were used for land use change scenario as well as combined climate and land use change analysis.

3.3. Potential effect of climate change on components of hydrological cycle

The future temperature projection in the NRW showed an increasing trend compared to base period (Fig. 7a). The average annual temperature increased from 9.4 °C to 12.5 °C and 12.7 °C, displaying a 33.3%, and 35.7% increase compared to base period under RCP-4.5 and 8.5 scenarios, respectively. The annual temperature cycle showed a clear increasing trend in average monthly mean temperature compared to base period throughout the year. The seasonal analysis of different components of hydrological cycle and temperature shows the % of increase/decrease in each parameters compared to base period (Table 6). The seasonal analysis of temperature depicted the highest increase in temperature compared to base period (178.8% and 201.9% for RCP-4.5 and 8.5, respectively) to occur during winter while the least rise (16.8% and 17.9% for RCP-4.5 and 8.5, respectively) was during summer. Both annual and seasonal analysis demonstrated overall warming of the watershed with higher temperature under RCP-4.5 and 8.5 scenarios compared to base period.

The future precipitation projection in the NRW showed a slight decreasing trend compared to base period (Fig. 7 b). Overall, the average annual precipitation in the NRW decreased from 107.57 mm to 102.95 mm and 103.79 mm, representing a 4.3% and 3.5% decrease compared to base period under RCP-4.5 and 8.5 scenarios, respectively. The annual precipitation cycle remained unchanged from January to May while a shift in precipitation cycle was observed from June to December. The most notable differences were a shift of precipitation peak from June to August accompanied by a sharp decline in precipitation until October. The seasonal analysis of precipitation depicted the highest reduction in precipitation (7.48% and 7.73% for RCP-4.5 and 8.5, respectively) during fall while the least reduction in spring season (1.22% and 0.56% for RCP-4.5 and 8.5, respectively). Shifting of this precipitation pattern accompanied with rising temperature may increase the risk of drought, flooding, and water quality degradation in the watershed (Mishra and Liu, 2014; Wu et al., 2012b). The findings of increasing temperature and lesser precipitation in the future projected scenarios is consistent with the results of other researchers including Paul et al. (2017), Neupane and Kumar (2015), and Jha et al. (2007).

In response to an increased temperature and reduced precipitation in the watershed, the snowfall decreased throughout the year for the future climate change under both RCP-4.5 and 8.5 scenarios compared to base period (Fig. 7c). The average annual snowfall reduced from 12.70 mm to 6.40 mm and 5.96 mm which depicts a decrease in nearly 50% and 53% compared to base period under RCP-4.5 and 8.5 scenarios, respectively.

As a result of decrease in snowfall and precipitation for future climate change scenarios under RCP 4.5 and 8.5 compared to base period, a decline in surface runoff was observed during most months except for August and November (Fig. 7 d). The increased surface runoff during these two months was due to higher precipitation in both RCPs compared to base period (Fig. 7b). The mean annual surface runoff decreased from 29.60 mm (base period) to 22.32 mm (RCP-4.5 and 8.5) which represents a 24.40% reduction. A similar reduction in surface runoff was observed by Culbertson et al. (2016) in Maumee River Watershed in Ohio, United States under RCP-4.5 and 8.5 scenarios. The seasonal analysis indicates that the maximum surface runoff reduction was observed during summer while the minimum reduction was found during fall (Table 6).

Despite lower precipitation, higher streamflow was observed in the watershed for both climate change RCP scenarios compared to base period (Fig. 7 e) due to higher yield (Fig. 7 f). The higher yield was contributed by higher groundwater (Fig. 7 g) and lateral flow (Fig. 7 h) in both RCPs compared to base period. The higher groundwater and lateral flow may be due to increase in infiltration capacity of soil due to increase in air temperature in future climate change. Increasing air temperature leads to frost free soil in most of the year which increases soil temperature, the resultant impact increases soil pore water holding capacity leading to higher soil hydraulic conductivity which results into higher infiltration and less surface runoff (Pradhan et al., 2019; Stähli et al., 1999; Dunne and Black, 1971). A similar result was also observed in the future climate change scenario by Culbertson et al.(2016) in the Maumee River Watershed, Ohio. Additionally, Pervez and Henebry (2015) found the increasing trend of lateral flow under climate change in the Brahmaputra River Basin in South Asia. The average annual streamflow increased from 2.21 m^3/sec (base line) to 2.92 m^3/sec and 2.93 m^3/sec (RCP-4.5 and RCP-8.5, respectively) which represents an increase in streamflow of approximately 32% in both RCPs compared to base period. The streamflow was correlated with water yield from both RCPs in the watershed. The annual water yield was 40.65 mm for the base period while it was 53.67 mm and 53.76 mm for RCP-4.5 and RCP-8.5, respectively. This indicates an approximately 32% increase in water yield in both RCPs compared to base period. A negligible difference in results between both RCPs may be due to consideration of future climate change in the near term (2020–2045) in this study. The increase in streamflow and water yield in both RCPs were consistent

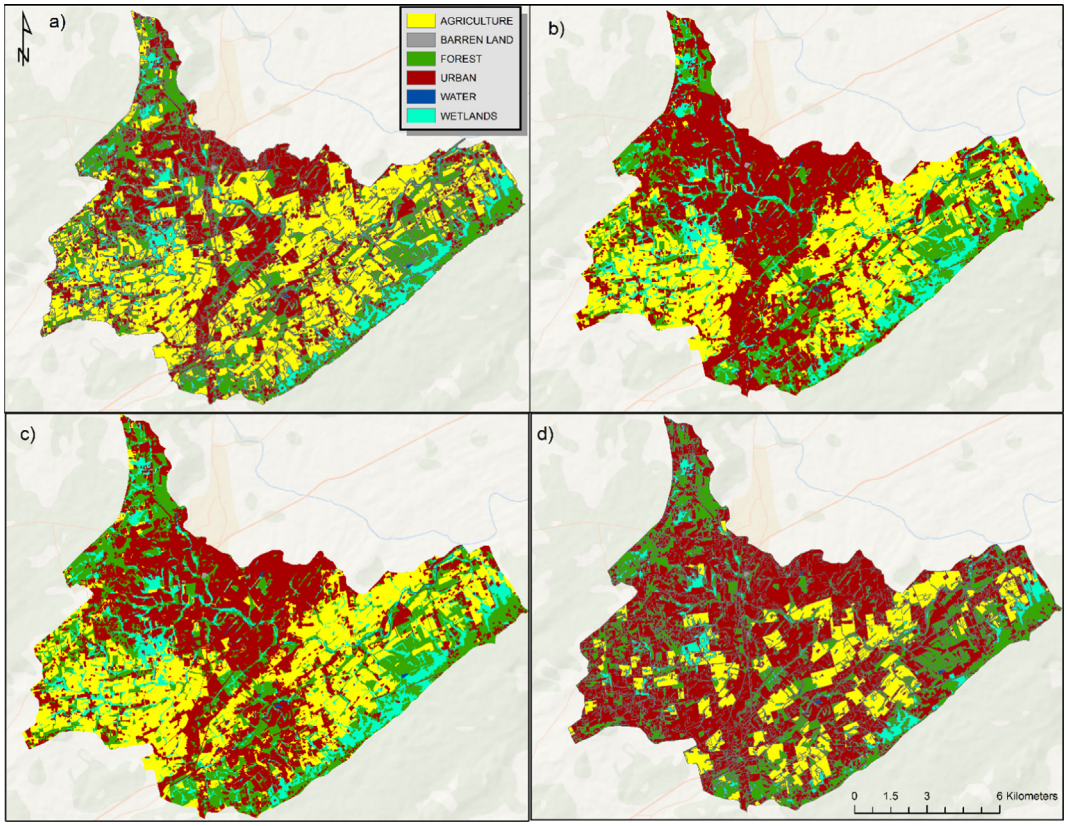

Fig. 6. Representation of land use in the Neshanic River Watershed based on (a) current-2012, (b) MLP-2040, (c) Simweight-2040, and (d) ABM-2040.

which was evident from the result. A 32% increase in streamflow due to water yield may potentially elevate the flooding risk in the watershed. Similar to the average annual streamflow and water yield, similar seasonal trends were observed between the two where maximum increase was found during fall and the minimum increase was noticed during winter (Table 6). A higher groundwater was predicted throughout the year for both RCPs compared to base period (Fig. 7 g). In fact, an average increase in more than 200% of groundwater was predicted for climate change under both RCPs compared to base period. This result may be due to substantial reduction in snowfall in the watershed which resulted in reduction of surface runoff events during winter and spring while facilitating infiltration. Furthermore, increasing projected temperature increases soil temperature leading to higher infiltration during the winter months (Culbertson et al., 2016). This indicates the critical role of groundwater towards streamflow in the watershed especially during low flow condition (summer season). However, a detail analysis of groundwater components in the watershed is required to assure the contribution of groundwater to streamflow. A similar increasing trend of groundwater was observed due to climate change in the Batsto River Watershed located in the Southern New Jersey (Daraio,2017). Similar to groundwater, an increasing trend of lateral flow was predicted throughout the year (Fig. 7 h). Approximately, more than 95% increase in average annual lateral flow was predicted in both RCPs compared to base period. The seasonal analysis suggests that the maximum increase in lateral flow was during fall while the minimum increase was during winter (Table 6). Daraio (2017) observed increased streamflow due to climate change in the Maurice River Watershed and Batsto River Watershed located in the Southern New Jersey. Similarly, Wagena and Easton (2018) reported an increase of streamflow in the range of 4.5–9% in the Susquehanna River Basin located in Chesapeake Bay due to climate change. Additionally, Hayhoe et al.(2013) found a positive shift in streamflow(by 5–10%) in the river basins located in the northeast United States as a result of climate change. Furthermore, Ahiablame et al. (2017) predicted the increase in streamflow between 8 and 48% by midcentury in the James River Watershed located in North and South Dakota, United States. Additionally, increase in streamflow was projected by other researchers due to future climate change including Shrestha and Wang (2017), Wagena et al. (2016), and Pervez and Henebry (2015) in different parts of the world.

The evapotranspiration was projected to decrease substantially throughout the year due to climate change (Fig. 7 i). The average 12-month annual evapotranspiration was approximately 65 mm and 48 mm for base period and climate change RCPs, respectively. This indicates that the evapotranspiration was projected to decrease by at least 25% in both RCPs compared to base period. The reduction in evapotranspiration was primarily be due to lower future precipitation (Neupane and Kumar, 2015; Kim et al., 2013) and this decreased evapotranspiration could have increased soil water and percolation (Fig. 7 j and k) in the watershed for climate change under both RCPs. The seasonal analysis depicts that the projected evapotranspiration was least during winter while it was highest during summer. In contrast to evapotranspiration, the average annual soil water and percolation were projected to increase by more than 52% and 180%, respectively in both RCPs compared to base period. The increase in soil water will reduce irrigation for different crop production in the watershed while increase in percolation will increase the groundwater recharge and ultimately increases streamflow. Paul et al. (2017) and Neupane and Kumar (2015) also found increased in soil water content and percolation, and decrease in evapotranspiration in their climate change studies in different watersheds in the United States.

Additionally, the long term monthly as well as seasonal trends of precipitation, streamflow, and sediment transport during the base period (1991–2015) in the NRW is presented in Section 3.2 of the Supplementary Material.

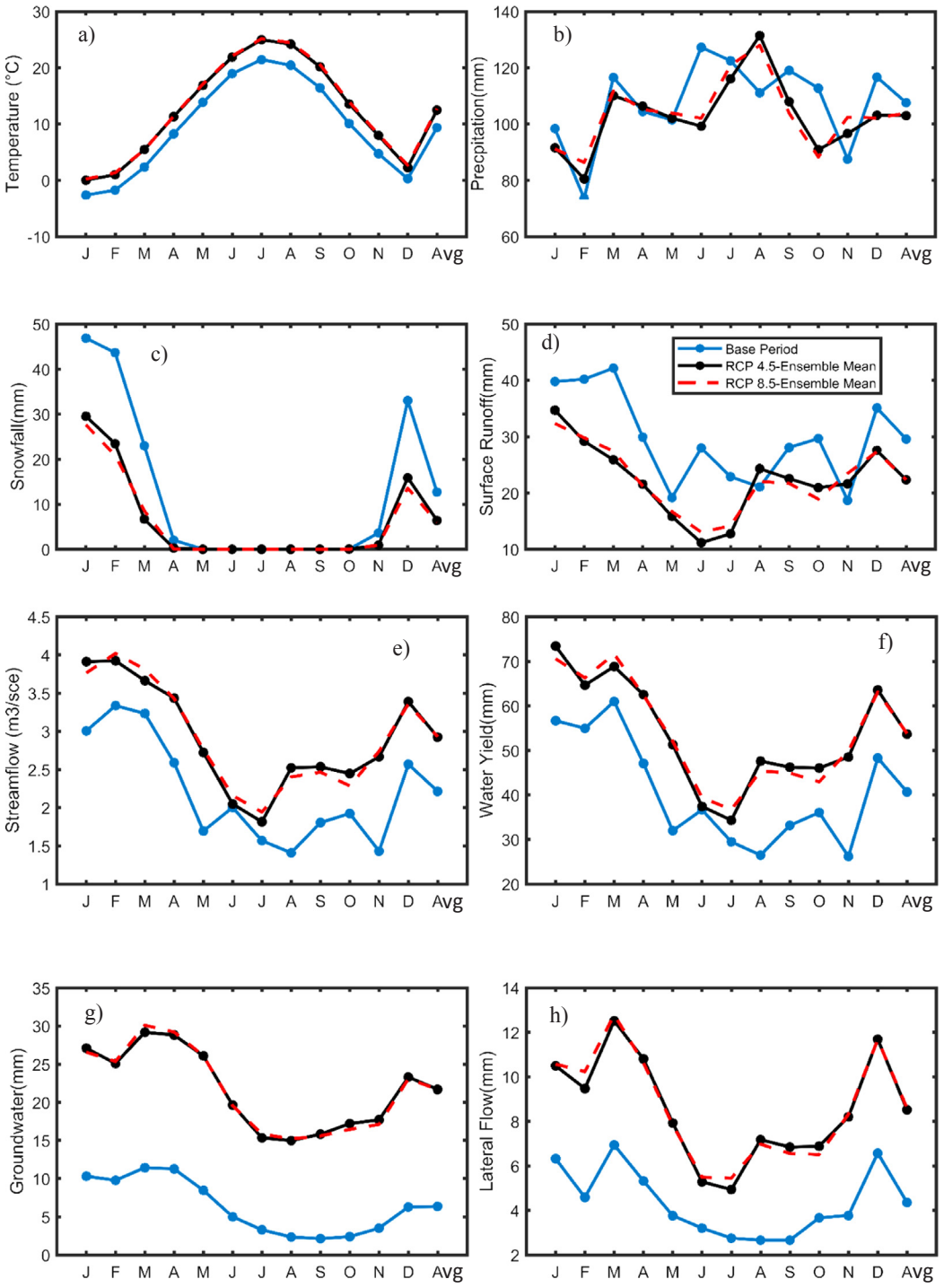

Fig. 7. Average monthly and annual mean of different components of hydrological cycle as well as sediment yield in the Neshanic River Watershed. In the figure caption, x axis represents month from January (J) to December (D) and the Avg stands for average of 12 months.

3.4. Consequence of climate change on sediment generation and sediment load in the watershed

To assess the impact of climate change on sediment production at subbasin level, SYLD of output.SUB file was used which depicts the weighted average of sediment from all HRUs within each subbasin before channel routing. In the base period condition, greater sediment yield was observed at southeast edge of the watershed while low-ersediment yield was found at north central side of the watershed (Fig. 8a). Under RCP-4.5, the majority of subbasins were predicted to have reduced sediment yield (Fig. 8b). The spatial pattern of sediment generation/reduction under RCP-8.5 was similar to RCP-4.5 except slightly more sediment generation subbasins were predicted (Fig. 8c). As might be expected, the spatial distribution of sediment yield among the subbasins was primarily dependent on topographic elevation of the watershed. For example, the higher sediment yield was predicted at the southeast as well as northwest subbasins in the watershed having steeper slopes compared to other parts (Figs. 1 and 8 b). In contrast, negative sediment generation was forecasted in most of the subbasins located in the center of the watershed having lesser topographic elevation. Additionally, most of the subbasins generating higher sediment yield also displayed increasing surface runoff under the climate change

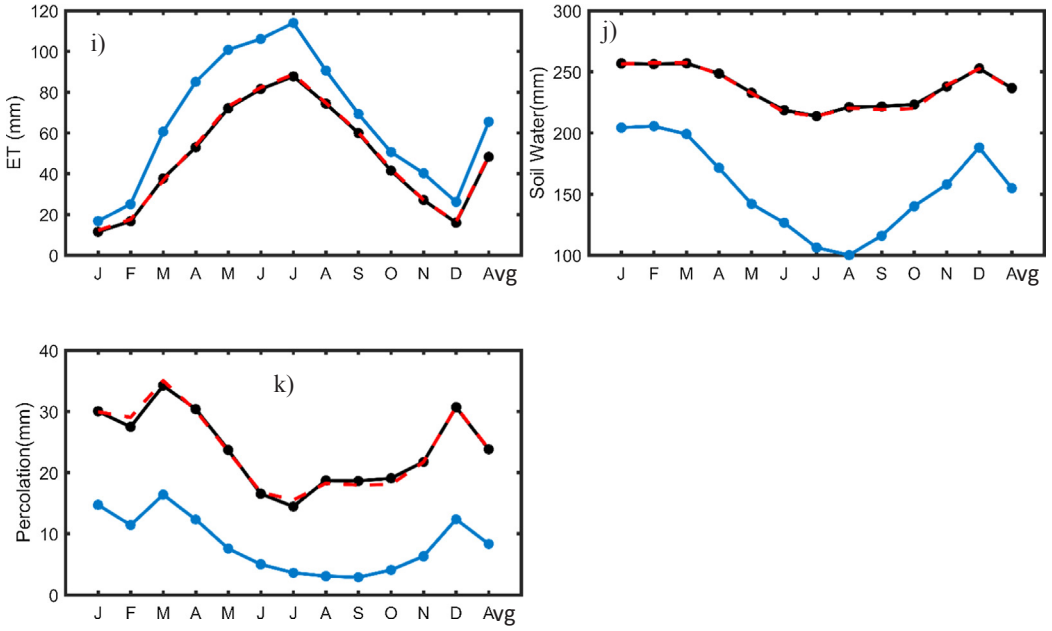

Fig. 7. (*continued*)

scenarios compared to base period (Fig. S6, Supplementary Material). Shrestha and Wang (2018) also found highest sediment generation in subbasins having steepest topography compared to other parts of the watershed using SWAT model during climate change study in Canada.

However, when sediment load was compared at the watershed outlet after considering channel routing, a slight increase in sediment load (more than 10%) compared to base period was observed for both RCPs in climate change scenario (Fig. 9). This increase can be attributed to greater channel and stream bed erosion due to higher streamflow (approximately 32%) in the climate change scenarios compared to the base period. Our findings are corroborated by the outcomes of previous study in the same watershed by Qiu and Wang (2014). They found that streams are the primary sources of sediment compared to different land uses contributing nearly 60% of the sediment load in the watershed. Furthermore, the monthly as well as seasonal trends between streamflow and sediment load during the base period (1991–2015) shows that the streamflow is the primary driver of sediment generation in the river (Fig. S5, Supplementary Material). When both RCPs were compared, RCP-8.5 produced slightly more sediment load compared to RCP-4.5 which may be due to greater numbers of sediment generation subbasins in RCP-8.5 compared to RCP-4.5 (Fig. 8 b and c). Overall, the climate change scenarios suggest increasing sediment load in the streams (Fig. 9) which may adversely affect the health of aquatic ecosystems. Wagena and Easton (2018) also found an increasing trend of annual sediment load ranging from 26 to 31% in the Susquehanna River Basin located in Chesapeake Bay due to climate change. Apart from sediment load, primary components of hydrologic cycle due to climate change only scenario compared to base period is also found from Fig. 9.

Table 6
Seasonal and annual percent change of hydrological components, temperature, and sediment yield from base period. (Winter: December-February, Spring: March-May, Summer: June-August, Fall: September-November).

Period	Temperature (%)		Precipitation (%)		Snowfall (%)		Surface runoff (%)	
	RCP-4.5	RCP-8.5	RCP-4.5	RCP-8.5	RCP-4.5	RCP-8.5	RCP-4.5	RCP-8.5
Winter	178.8	201.8	−4.6	−3.1	−44.3	−49.8	−20.5	–22.3
Spring	37.8	38.7	−1.2	−0.6	−72.3	−65.6	−30.7	−28.4
Summer	16.8	17.9	−3.9	−2.8			–33.0	−31.6
Fall	33.6	36.6	−7.5	−7.7	−74.4	−75.4	−14.8	−16.2
Annual	33.3	35.7	−4.3	−3.5	−49.6	−52.0	−24.5	−24.4
	Streamflow (%)		Water yield (%)		Groundwater (%)		Lateral flow (%)	
	RCP-4.5	RCP-8.5	RCP-4.5	RCP-8.5	RCP-4.5	RCP-8.5	RCP-4.5	RCP-8.5
Winter	25.0	25.1	26.1	25.0	186.3	184.5	81.2	85.9
Spring	30.7	33.1	30.4	32.9	169.9	174.2	95.0	95.1
Summer	28.2	30.6	28.8	31.2	371.1	377.2	101.9	108.0
Fall	48.3	45.2	47.5	44.4	533.8	513.9	117.3	111.8
Annual	32.1	32.3	32.0	32.2	241.9	241.8	95.8	97.4
	Evapotranspiration (%)		Soil water (%)		Percolation (%)			
	RCP-4.5	RCP-8.5	RCP-4.5	RCP-8.5	RCP-4.5	RCP-8.5		
Winter	−35.3	–32.4	28.0	28.1	129.0	133.0		
Spring	−34.0	–33.6	44.1	44.0	143.4	144.2		
Summer	−21.6	−20.9	96.2	95.5	325.0	332.5		
Fall	−19.8	−19.0	64.9	63.8	347.5	334.6		
Annual	−26.3	−25.5	52.9	52.5	186.3	187.3		

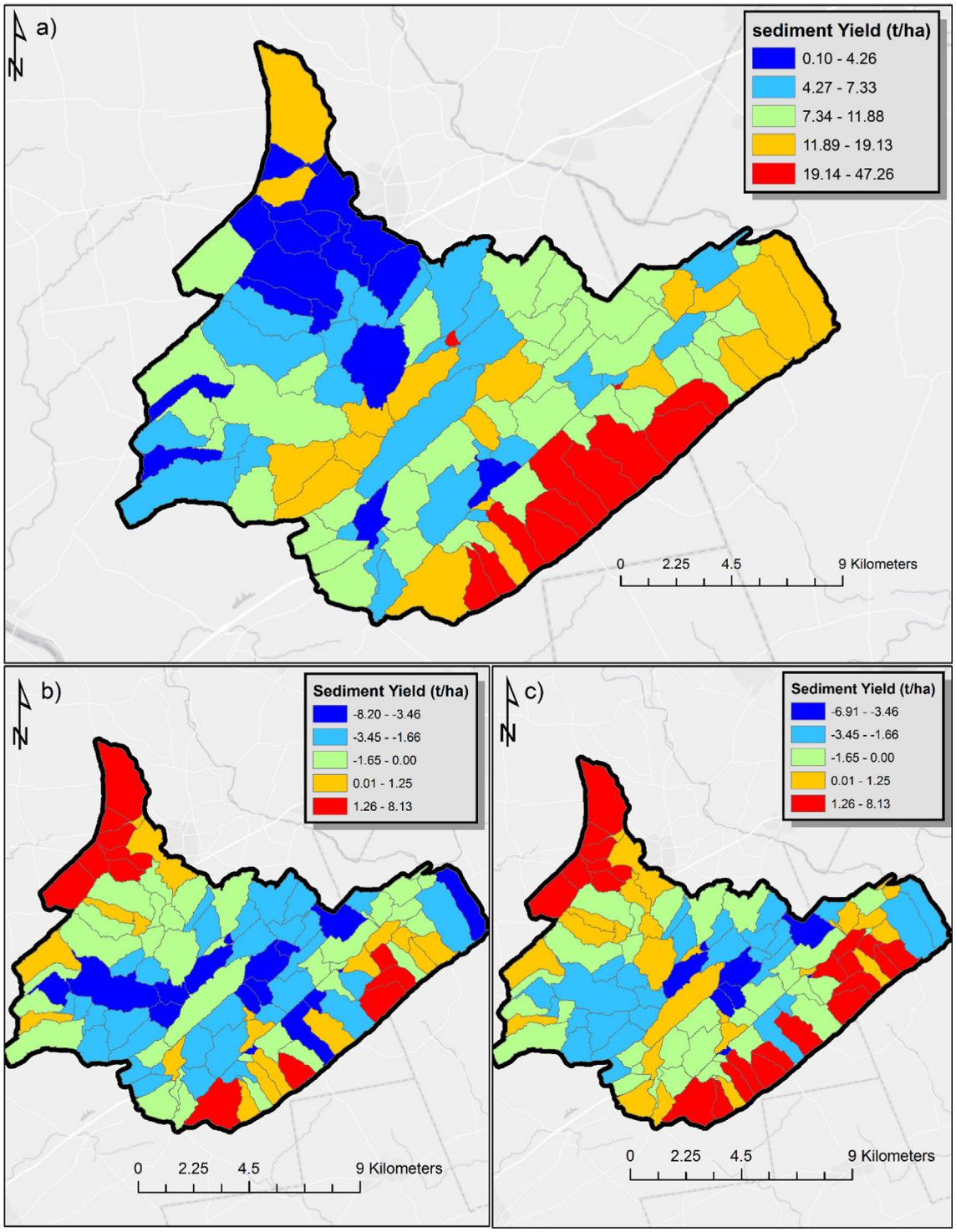

Fig. 8. Average annual sediment yield in fields in the Neshanic River Watershed: (a) Base line, (b) difference in sediment yield between RCP-4.5 and base line, and (c) difference in sediment yield between RCP-8.5 and base line.

3.5. Potential effect of land use change on components of hydrological cycles and sediment load

The land use change only based on ABM-2040 scenario projects an increase of 24% in urban land area leading to an increase in surface runoff (4%) (Fig. 10). Despite the increased surface runoff, a reduction in streamflow and water yield (approximately 5%) was forecastdue to reduction in both groundwater (by 39%) and lateral flow (18%).

This indicates the importance of subsurface flow in the watershed. The reduction in groundwater and lateral flow in the land use change scenario compared to base period was due to increase in impervious surface as a result of increased residential areas. A previous study of Giri et al.(2018) conducted in the same watershed where they forecasted water security based on projected land use of 2022 and found a similar result of increasing surface runoff and decreasing soil moisture pattern compared to base period due to lesser infiltration as a result of urbanization. The evapotranspiration was projected to decline due to conversion of a significant area of the agricultural lands and forest into

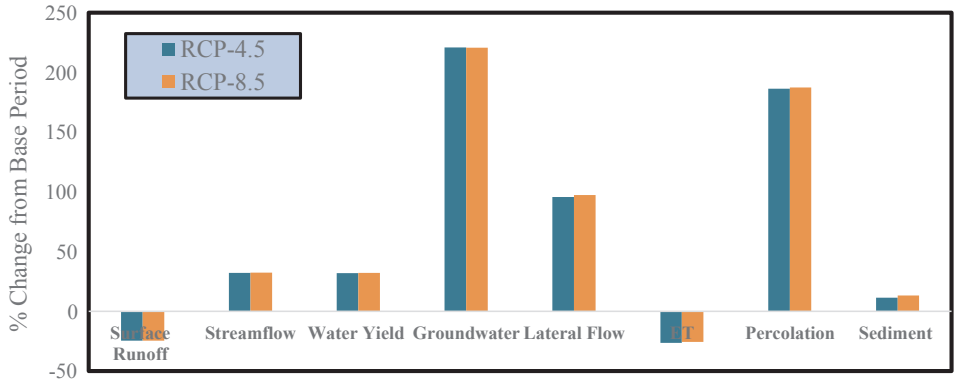

Fig. 9. Comparison of primary components of hydrological cycle and sediment load in the climate change only scenario compared to base period in the Neshanic River Watershed.

residential area even though additional lawns in the new residential areas were taken into account while estimating evapotranspiration. A similar decreasing trend of evapotranspiration was observed compared to base period due to conversion of agricultural lands and forest into residential areas in the same watershed for land use projected scenario of 2022 (Giri et al.,2018). Additionally, a reduction in percolation was observed in the land use change scenario compared to base period. Finally, approximately 42% reduction in sediment load was predicted in the land use change scenario compared to base period due to conversion of 2,785 ha agricultural lands (Table 5) into residential areas in the land use change scenario.

3.6. Potential effect of combined climate and land use change on components of hydrological cycles and sediment load

The trends of different components of hydrological cycles and sediment load for the combined climate and land use change scenario are similar to the trends found in the climate change only scenario. When each components were compared among two emission scenarios (RCP-4.5 and RCP-8.5), a negligible difference was observed between the two emission scenarios.

The surface runoff in the combined climate and land use change scenario was projected to decrease around 4% compared to base period (Fig. 11). Despite increased impervious surface through increased residential area, lesser runoff was predicted due to lower projected precipitation in the combined climate and land use change scenario compared to base period. This indicates that climate (i.e. reduced precipitation) has greater contribution on hydrologic process compared to land use. Despite lower surface runoff, higher streamflow and water yield (36%) was predicted in the combined climate and land use change scenario due to higher increase in groundwater, lateral flow, and percolation. Evapotranspiration was projected to decrease approximately 24% under combined climate and land use change scenario compared to base period. This result was due to conversion of agricultural land and forest into residential area combined with lesser precipitation.

Finally, the sediment load in the watershed was predicted to decrease roughly 30% in the combined climate and land use scenario compared to base period which was due to conversion of most of the agricultural lands towards urban land plus lesser surface runoff. The reduction of sediment in this scenario was lower compared to land use change alone due to offset of sediment reduction by climate change in the coupled climate and land use change scenario.

3.7. Summary of results across all three scenarios

A composite summary of primary components of three scenarios compared to base period is presented in Table 7. The ensemble GCM predicts warmer temperatures and declining snowfall and precipitation amounts leading to a projected decrease in surface runoff (as modeled in SWAT) in climate change only scenario. Conversely, an increasing surface runoff trend was predicted for the land use change scenario due to an increase in impervious surface area. When modeled in composite, the increased impervious surface from new urban lands was compensated for by the reduction in surface runoff in the climate change scenario. Streamflow and water yield are predicted to increase in the future despite decreased precipitation and surface runoff due to an increase in percolation and lateral flow compared to base period in both climate change alone as well as combined climate and land use change

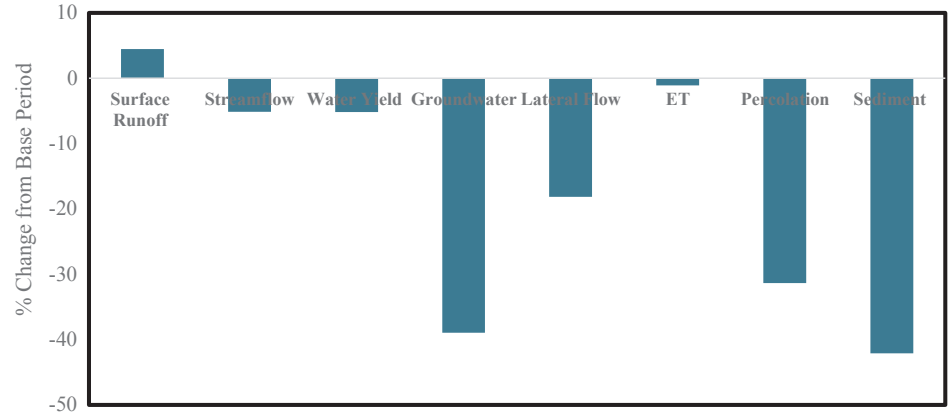

Fig. 10. Comparison of different components of hydrological cycle and sediment load in the land use change scenario compared to base period in the Neshanic River Watershed.

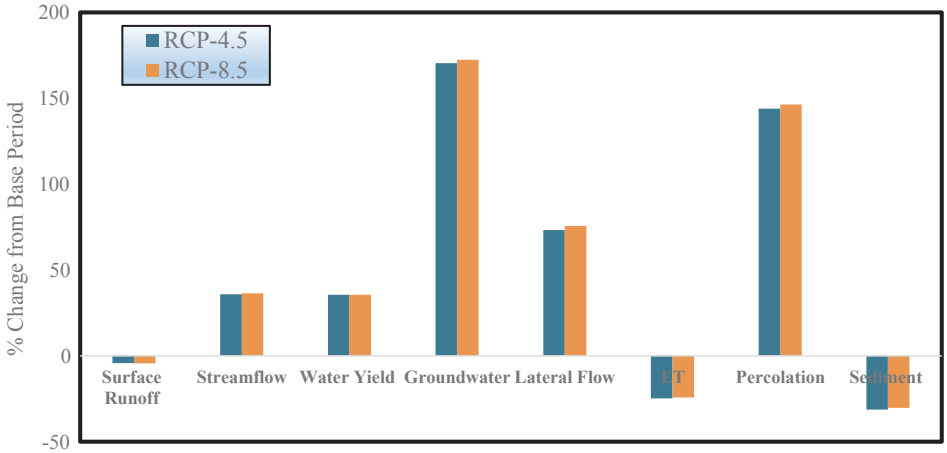

Fig. 11. Comparison of different components of hydrological cycle and sediment load in the combined climate and land use change scenario compared to base period in the Neshanic River Watershed.

scenario.

These results suggest the importance of sub-surface flow in the watershed. Similar relationships of streamflow versus surface runoff and subsurface flow were observed by Culbertson et al. (2016) and Neupane and Kumar (2015) in climate change study in Ohio and South Dakota watersheds, respectively.

The projected sediment load was slightly greater in climate change only scenario compared to the base period which may be attributed to channel erosion due to increase in streamflow. However, an opposite trend of decreasing sediment load was predicted in both land use change only as well as combined climate and land use change scenario likely due to the extensive conversion of agricultural lands into residential areas.

4. Conclusions

Understanding the standalone as well as combined effects of climate change and land use transformation are needed to formulate better water resource management and adaptation strategies in a changing environment. The integrated modeling framework we have developed facilitates the assessment of the potential impact of climate and land use change, either in isolation or in composite, on different components of hydrological cycle and sediment loading.

We suggest that streamflow and sediment load serve as suitable metrics for assessing watershed resilience, whether due to changing climate or land use. Our results predict the changing climate will have a larger effect on the hydrologic cycle than intensifying urban land uses in our study watershed. The coupled hydrologic-land use change modeling suggests increasing urbanization will result in lower streamflow. The climate change scenarios, either alone or in composite with land use change, predict higher streamflow; overriding the effect of land use changes. In our study watershed, higher levels of streamflow will likely exacerbate existing flooding issues and thereby serve to lower watershed resiliency. Conversely, the climate and land use change scenarios predict opposite effects on sediment load with the climate change increasing sediment loading to the study watershed. When modelled in composite, the effect of changing land use (in this case the conversion of erodible agricultural fields to suburban development) overrides the adverse effect of climate change, enhancing watershed resiliency by reducing sediment load and thereby improving health of the downstream aquatic ecosystems.

The integrated modeling framework we have developed is transferable to other watersheds providing practitioners a more effective way to examine the implications of land use and climate change, either alone or in composite.

Acknowledgements

The research was supported by the Johnson Family Chair in Water Resources & Watershed Ecology and the Sustainable Raritan River

Table 7
A composite summary of primary hydrological cycle components and sediment load from three scenarios in the Neshanic River Watershed. Where ↑ represents increasing trend compared to base period while ↓ represents decreasing trend.

Parameters	Climate Change	Land use Change	Combine Climate and Land Use Change
Surface runoff	↓	↑	↓
Streamflow	↑	↓	↑
Water yield	↑	↓	↑
Groundwater	↑	↓	↑
Lateral flow	↑	↓	↑
Evapotranspiration	↓	↓	↓
Sediment load	↑	↓	↓

Initiative at Rutgers University. We gratefully acknowledge the World Climate Research Programme's Working Group on Coupled Modeling, and we also gratefully thank the Climate Modeling Groups listed in Table S1 for producing and making available their model out. For CMIP the U.S. Department of Energy's Program for Cli-mate Model Diagnosis and Intercomparison provides coordinating support and led development of software infrastructure in partnership with the Global Organization for Earth System Science Portals. Additionally, we would like to thank Mr. Srinivas Gaddam for helping in making some figures for this manuscript.

Appendix A. Supplementary data

Supplementary data to this article can be found online at https://doi.org/10.1016/j.jhydrol.2019.123955.

References

Abbaspour, K.C., Johnson, C.A., van Genuchten, M.T., 2004. Estimating uncertain flow and transport parameters using a sequential uncertainty fitting procedure. Vadose Zone J. 3 (4), 1340–1352.

Abbaspour, K.C., Vejdani, M., Haghighat, S., 2007. SWAT-CUP calibration and uncertainty programs for SWAT. Modsim 2007: International Congress on Modelling and Simulation: Land, Water and Environmental Management: Integrated Systems for Sustainability, Christchurch, New Zealand.

Abbaspour, K.C., 2012. SWAT-CUP 2012: SWAT Calibration and Uncertainty Programs – A User Manual. Swiss Federal Institute Science and Technology, Eawag.

Ahiablame, L., Sinha, T., Paul, M., Ji, J., Rajib, A., 2017. Streamflow response to potential land use and climate changes in the James River Watershed, upper Midwest United States. J. Hydrol. Regional Studies 14, 150–166.

Arbab, Nazia N., 2014. Application of a Spatially Explicit, Agent-Based Land Use Conversion Model to Assess Water Quality Outcomes under Buffer Policies. (PhD dissertation). West Virginia University.

Arbab, N., Collins, A.R., Conley, J., 2016. Projections of watershed pollutant loads using a spatially explicit, agent-based land use conversion model: a case study of Berkeley County, West Virginia. Appl. Spat. Anal. Polic. https://doi.org/10.1007/s12061-016-9197-z.

Arbab, N., Hartman, J., Quispe, J., Grabosky, J., 2019. Implications of Different DEMs on Watershed Runoffs Estimations. J. Water Resource Protection 11, 448–467. https://doi.org/10.4236/jwarp.2019.114027.

Arnold, J.G., Srinivasan, R., Muttiah, R.S., Williams, J.R., 1998. Large area hydrologic modeling and assessment Part I: model development. J. Am. Water Resour. Assoc. 34, 73–89.

Arsanjani, J.J., Helbich, M., Kainz, W., Darvishi, A.B., 2013. Integration of logistic regression, Markov chain and cellular automata models to simulate urban expansion - the case of Tehran. Int. J. Appl. Earth Obs. 21, 265–275.

Atkinson, P.M., Massari, R., 1998. Generalized linear modeling of susceptibility to landsliding in the central Apennines. Italy. Comput. Geos. 24, 373–385.

Barton, C.V.M., et al., 2012. Effects of elevated atmospheric CO2 on instantaneous transpiration efficiency at leaf and canopy scales in Eucalyptus saligna. Glob. Chang. Biol. 18 (2), 585–595.

Boe, J., Terray, L., Martin, E., Habets, F., 2009. Projected changes in components of the hydrological cycle in French river basins during the 21st century. Water Resour. Res. 45, W08426.

Babamaaji, R.A., 2013. Impaxts of precipitation, land use, land cover, and soil type on the water balance of Lake Chand basin. Doctoral Dissertation, University of Missouri, Kansas City. Available at: http://citeseerx.ist.psu.edu/viewdoc/download?doi=10.1.1.854.6273&rep=rep1&type=pdf. (accessed 07.03.2018).

Batty, M., 2012. A generic framework for computational spatial modeling. In: Heppenstall, A.J., Crooks, A.T., See, L.M., Batty, M. (Eds.), Agent-based models of geographical systems. Springer, New York, NY, pp. 19–50.

Benenson, I., Torrens, P., 2004. Geosimulation: Automata-based modeling of urban phenomena. Wiley, West Sussex.

Bhatti, S.S., Tripathi, N.K., Nitivattananon, V., Rana, I.A., Mozumder, C., 2015. A multiscale modeling approach for simulating urbanization in a metropolitan region. Habitat Int. 50, 354–365.

Brekke, L., Thrasher, B.L., Maurer, E.P., Pruitt, T., 2013. Downscaled CMIP3 and CMIP5 climate projection. Release of downscaled CMIP5 climate projections, comparision with proceeding information, and summary of users needs. Bureau of Reclamation.

Bussi, G., Dadson, S.J., Prudhomme, C., Whitehead, P.G., 2016. Modelling the futre impacts of climate and land use change on suspended sediment transport in the River Thames(UK). J. Hydrol. 542, 357–372.

Camacho Olmedo, M.T., Paegelow, M., Mas, J.F., 2013. Interest in intermediate soft classified maps in land change model validation: suitability versus transition potential. Int. J. Geogr. Inf. Sci. 27 (12), 2343–2361.

Chen, Y., Ale, S., Rajan, N., Srinivasan, R., 2017. Modeling the effects of land use change from cotton (Gossypium hirsutum L.) to perinnial bioenergy grasses on watershed hydrology and water quality under changing climate. Agr. Water Manage. 192, 198–208.

Chien, H., Yeh, P.J.F., Knouft, J.H., 2013. Modeling the potential impacts of climate change on streamflow in agricultural watersheds of the Midwestern United States. J. Hydrol. 491, 73–88.

Cho, J., Barone, V.A., Mostaghimi, S., 2009. Simulation of land use impacts on groundwater levels and streamflow in a Virginia watershed. Agric. Water Manag. 96 (1), 1–11.

Cousino, L.K., Becker, R.H., Zmijewski, K.A., 2015. Modeling the effects of climate change on water, sediment, and nutrient yields from the Maumee River Watershed. J. Hydrol. 4, 762–775.

Clark Labs. 2018. TerrSet, Clark University. Available at: http://www.clarklabs.org/. (accessed 18.06.2018).

Culbertson, A.M., Martin, J.F., Aloysius, N., Ludsin, S.A., 2016. Anticipated impacts of climate change on 21st century Maumee River discharge and nutrient loads. J. Great Lakes Res 42, 1332–1342.

Daraio, J.A., 2017. Potential climate change impacts on streamflow and recharge in two watersheds on the New Jersey Coastal Plain. J. Hydrol. Eng. 22, 1–18.

Dendoncker, N., Rounsevell, M., Bogaert, P., 2007. Spatial analysis and modelling of land use distributions in Belgium. Comput. Environ. Urban. 31 (2), 188–205.

Dunne, T., Black, R.D., 1971. Runoff processes during snowmelt. Water Resour. Res. 7, 1160–1172.

Ficklin, D., Barnhart, B.L., 2014. SWAT hydrologic model parameter uncertainity and its implications for hydroclimatic projections in snowmelt dependent watersheds. J. Hydrol. 519, 2081–2090.

Fix, E., Hodges, J. L., 1951. Discriminatory analysis, nonparametric discrimination: consistency properties. Project No. 21-49-004, Report No. 4 USAF School of Aviation Medicine, Randolph Field, Texas, USA.

Folke, C., 2006. Resilience: The emergence of a perspective for social-ecological systems analyses. Global Environ. Chang. 16, 253–267.

Frumhoff, P.C., McCarthy, J.J., Melillo, J.M., Moser, S.C., Wuebbles, D.J., 2007. Confronting climate change in the US Northeast. Science, impacts, and solutions. Available at: https://www.ucsusa.org/sites/default/files/legacy/assets/documents/global_warming/pdf/confronting-climate-change-in-the-u-s-northeast.pdf. (accessed 18.06.2018).

Gabriel, M., Knightes, C., Cooter, E., Dennis, R., 2016. Evaluating relative sensitivity of SWAT simulated nitrogen discharge to projected climate and land cover changes for two watersheds in North Carolina. USA. Hydrol. Process. 30, 1403–1418.

Gassman, P.W., Reyes, M.R., Green, C.H., Arnold, J.G., 2007. The soil and water assessment tool: historical development, applications, and future research directions. Trans. ASABE 50, 1211–1250.

Giri, S., Nejadhashemi, A.P., Woznicki, S., 2012. Evaluation of targeting methods for implementation of best management practices in the Saginaw River Watershed. J. Environ. Manage. 103, 24–40.

Giri, S., Nejadhashemi, A.P., Woznicki, S.A., Zhang, Z., 2014. Analysis of best management practice effectiveness and spatiotemporal variability based on different targeting strategies. Hydrol Process. 28, 431–445.

Giri, S., Nejadhashemi, A.P., Zhang, Z., Woznicki, S.A., 2015. Integrating statistical and hydrological models to identify implementation sites for agricultural conservation practices. Environ. Modell. Softw. 72, 327–340.

Giri, S., Qiu, Z., Prato, T., Luo, B., 2016a. An integrated approach for targeting critical source areas to control nonpoint source pollution in watersheds. Water Resour. Manage. 30, 5087–5100.

Giri, S., Krasnuk, D., Lathrop, R. G., Malone, S. J., Herb, J., 2016b. State of the Raritan Report, Volume 1, Sustainable Raritan River Initiative, Rutgers University, 2016. Available at: http://raritan.rutgers.edu/wp-content/uploads/2017/01/SOR-Final2017-01-30.pdf. (accessed 18.06.2018).

Giri, S., Arbab, N.N., Lathrop, R.G., 2018. Water security assessment of current and future scenarios through an integrated modeling framework in the Neshanic River Watershed. J. Hydrol. 563, 1025–1041.

Guan, D.J., Li, H.F., Inohae, T., Su, W.C., Nagaie, T., Hokao, K., 2011. Modeling urban land use change by the integration of cellular automata and Markov model. Ecol. Model. 222, 3761–3772.

Hagerstrand, T., 1965. A Monte Carlo approach to diffusion. Archive of European Sociology, VI, pp. 43–67.

Hayhoe, K., Stoner, A., Gelca, R., 2013. Climate change projections and indicators for Delaware. Available at: http://www.dnrec.delaware.gov/energy/Documents/Climate%20Change%202013-2014/ARC_Final_Climate_Report_Dec2013.pdf. (accessed 28.3.2019).

Immerzeel, W., 2008. Historical trends and future predictions of climate variability in the Brahmaputra basin. Int. J. Climatol. 28, 243–254.

IPCC, 2014. Climate Change 2014: Impacts, Adaptation, and Vulnerability. Part A:Global and Sectoral Aspects. Contribution of Working Group II to the FifthAssessment Report of the Intergovernmental Panel on Climate Change.Cambridge University Press, Cambridge, United Kingdom/New York, NY,USA.

Jensen, N.H., Veihe, A., 2009. Modelling the effect of land use and climate change on the water balance and nitrate leaching in eastern Denmark. J. Land Use Sci. 4, 53–72.

Jha, M., Arnold, J.G., Gassman, P.W., Giorgi, F., Gu, R.R., 2007. Climate change sensitivity assessment on upper Missisipi river basin streamflows using SWAT. J. Am. Water Resour. Assoc. 42 (4), 997–1015.

Karlsson, I.B., Sonnenborg, T.O., Seaby, L.P., Jensen, K.H., Refsgaard, J.C., 2015. Effect of a high-end CO2-emission scenario on hydrology. Clim. Res. 64, 39–54.

Kim, H.K., Parajuli, P.B., Filip To, S.D., 2013. Assessing impacts of bioenergy crops and climate change on hydrometeorology in the Yazoo River Basin. Mississippi. Agric. For. Meteorol. 169, 61–73.

Kundzewicz, Z.W., Mata, L.J., Arnell, N.W., Döll, P., Kabat, P., Jiménez, B., Miller, K.A., Oki, T., Sen, Z., Shiklomanov, I.A., 2007. Freshwater resources and their management. In: In: Parry, M.L., Canziani, O.F., Palutikof, J.P., Van der Linden, P.J., Hanson, C.E. (Eds.), Climate Change 2007: Impacts, Adaptation and Vulnerability.

Contribution of Working Group II to the Fourth Assessment Report of the Intergovernmental Panel on Climate Change Cambridge University Press, Cambridge, UK, pp. 173–210.
Labat, D., Godderis, Y., Probst, J.L., Guyot, J.L., 2004. Evidence of global runoff increase related to climate warming. Adv. Water Resour. 27, 631–642.
Lathrop, R.G., Bognar, J.A., Hasse, J.E., 2016. Changing landscapes in the Garden Sate. Available at: http://www.crssa.rutgers.edu/projects/lc/download/NJ_Urb_Growth_III_executive_summary_2012_LathropHasse.pdf. (accessed 18.06.2018).
Lee, S., 2005. Application of logistic regression model and its validation for landslide susceptibility mapping using GIS and remote sensing data. Int. J. Remote Sens. 26 (7), 1477–1491.
Love, B.J., Nejadhashemi, A.P., 2011. Water quality impact assessment of large scale biofuel crops expansion in agricultural regions of Michigan. Biomass Bioenerg. 35, 2200–2216.
Luo, Y., Ficklin, D.L., Liu, X., Zhang, M., 2013. Assessment of climate change impacts on hydrology and water quality with a watershed modeling approach. Sci. Total Environ. 450–451, 72–82.
Ma, X., Xu, J., Luo, Y., Aggarwal, S.P., Li, J., 2009. Response of Hydrological Processes to Land-Cover and Climate Changes in Kejie Watershed, Southwest China. Hydrol. Process. 23, 1179–1191.
Mao, D., Cherkauer, K.A., 2009. Impacts of land-use change on hydrologic responses in the Great Lakes region. J. Hydrol. 374 (71–82), 2009.
Mas, J.F., Kolb, M., Paegelow, M., Teresa, M., Camacho Olmedo, M.T., Houet, T., 2014. Inductive pattern-based land use/cover change models: A comparison of four software packages. Environ. Modell. Softw. 51, 94–111.
Mehdi, B., Ludwig, R., Lehner, B., 2015. Evaluating the impacts of climate change and crop land use change on streamflow, nitrates and phosphorus: A modeling study in Bavaria. J. Hydrol. Regional Studies 4, 60–90.
Menard, S., 1995. Applied logistic regression analysis. Sage University Paper Series on Quantitative Applications in Social Sciences 106, 98.
Mishra, A., Liu, S.C., 2014. Changes in precipitation pattern and risk of drought over India in the context of global warming. J. Geophys. Res. Atoms. 119, 7833–7841. https://doi.org/10.1002/2014JD021471.
Molina-Navarro, E., Andersen, H.E., Nielsen, A., Thodsen, H., Trolle, D., 2018. Quantifying the combined effects of land use and climate changes on streamflow and nutrient loads: a modeling approach in the Odense Fjord catchment (Denmark). Sci. Total Environ. 621, 253–264.
Moriasi, D.N., Arnold, J.G., VanLiew, M.W., Binger, R.L., Harmel, R.D., Veith, V., 2007. Model evaluation guidelines for systematic quantification of accuracy in watershed simulations. Trans. ASABE 50, 885–900.
Mozumder, C., Tripathi, N.K., Losiri, C., 2016. Comparing three transition potential models: a case study of built-up transitions in north-east India. Comput Environ Urban Syst 59, 38–49. https://doi.org/10.1016/j.compenvurbsys.2016.04.009.
Mutenyo, I., Nejadhashemi, A.P., Woznicki, S.A., Giri, S., 2013. Evaluation of SWAT performance on amountaneous watershed in tropical Africa. Hydrol. Current Res S14. https://doi.org/10.4172/2157-7587.S14-001.
Nasiri, Vahid & Darvishsefat, Ali & Rafiee, Reza & Shirvany, Anoushirvan & Avatefi Hemat, Mohammad, 2018. Land use change modeling through an integrated Multi-Layer Perceptron Neural Network and Markov Chain analysis (case study: Arasbaran region, Iran). J. Forestry Res. 10.1007/s11676-018-0659-9.
National Conference of State legislatures (NCSL), 2008. Climate change and the economy, New Jersey, Assessing the costs of climate change. Avaialbale at: http://cier.umd.edu/climateadaptation/Climate%20change–NJ.pdf. (accessed 18.06.2018).
National Agricultural Statistics Service(NASS): CropScape- Cropland Data Layer, 2017. Available at: https://nassgeodata.gmu.edu/CropScape/. (accessed 05.04.18).
Neitsch, S.L., Arnold, J.G., Kiniry, J.R., Williams, J.R., 2011. Soil and Water Assessment Tool: Theoretical Documentation, Version 2009. Texas Water Resources Institute.
Nelson, D.R., Adger, W.N., Brown, K., 2007. Adaptation to environmental change: contributions of a resilience framework. Annu. Rev. Environ. Resour. 32, 395–419.
Neupane, R.P., Kumar, S., 2015. Estimating the effects of potential climate and land use changes on hydrologic processes of a large agriculture dominated watershed. J. Hydrol. 529, 418–429.
New Jersey Department of Environmental Protection (NJDEP), 2011. The Neshanic river restoration plan. Trenton, NJ. Available at: https://www.state.nj.us/dep/wms/bears/docs/1.0.%20Neshanic%20Plan.pdf. (accessed 18.06.2018).
New Jersey Department of Environmental Protection (NJDEP), 2012. Land use Land cover Classification Systems: NJDEP Modified Anderson Classification Systems. NJDEP, Trenton, NJ.
New Jersey Department of Environmental Protection (NJDEP), 2018. Bureau of GIS. NJDEP, Trenton, NJ. Available at: https://www.nj.gov/dep/gis/wmalattice.html. (accessed 15.05.2018).
Oñate-Valdivieso, F., Bosque Sendra, J., 2010. Application of GIS and remote sensing techniques in generation of land use scenarios for hydrological modeling. J. Hydrol. 395, 256–263.
Peng, J., Dan, L., Dong, W., 2014. Are there interactive effects of physiological and radiative forcing produced by increased CO2 concentration on changes of land hydrological cycle? Glob. Planet. Chang. 112, 64–78.
Pijanowski Bryan, C., Daniel G. Brown, Bradley A. Shellito, Gaurav A. Manik, 2002. Using neural networks and GIS to forecast land use changes: a Land Transformation Model, Computers, Environment and Urban Systems, 26(6), 553-575, ISSN 0198-9715, https://doi.org/10.1016/S0198-9715(01)00015-1.
Panagopoulos, Y., Gassman, P.W., Arritt, R.W., Herzmann, D.E., Campbell, T.D., Valcu, A., Jha, M.K., Kling, C.L., Srinivasan, R., White, M., Arnold, J.G., 2015. Impacts of climate change on hydrology, water quality and crop productivity in the Ohio-Tenessee River Basin. Int. J. Agric. Boil. Eng. 8, 36–53.
Paul, M., Rajib, M.A., Ahiablame, L., 2017. Spatial and temporal evaluation of hydrological response to climate and change in three South Dakota Watersheds. J. Am. Water Resour. As. 53, 69–88.
Pervez, M.S., Henebry, G.M., 2015. Assessing the impacts of climate and land use and land cover change on freshwater availability in the Brahamputra River Basin. J. Hydrol. Regional Studies 3, 285–311.
Pontius, R.G., Schneider, L.C., 2000. Land-use change model validation by a ROC method. Agric. Ecosyst. Environ. 85, 269–280.
Pontius Jr, R.G., Schneider, L.C., 2001. Land-cover change model validation by an ROC method for the Ipswich watershed, Massachusetts. USA. Agric. Ecosyst. Environ. 85 (1–3), 239–248.
Pijanowski, B.C., Tayyebi, A., Delavar, M., Yazdanpanah, M., 2009. Urban expansion simulation using geospatial information system and srtificial neural networks. Int. J. Environ. Res. 3 (4), 493–502.
Pradhan, N.R., Downer, C.W., Marchenko, S., 2019. Catchment hydrological modeling with soil thermal dynamics during seasonal freeze-thaw cycles. Water 11, 116. https://doi.org/10.3390/w11010116.
Praskievicz, S., Bartlein, P., 2014. Hydrologic modeling using elevationally adjusted NARR and NARCCAP regional climate-model simulations: Tucannon River, Washington. J. Hydrol. 517, 803–814.
Qiu, Z., Wang, L., 2014. Hydrological and water quality assessment in a suburban watershed with mixed land uses using the SWAT model. J. Hydrol. Eng. 19, 816–827.
Reshmidevi, T.V., Kumar, D.N., Mehrotra, R., Sharma, A., 2017. Estimation of the climate change impact on a catchment water balance using an ensemble of GCMs. J. Hydrol. 556, 1192–1204.
Runkel, R.L., Crawford, C.G., Cohn, T.A., 2004. LOAD ESTIMATOR (LOADEST): a fortan program for estimating constituent laods in streams and rivers. US geological survey techniques and methods book 4, Chap. A5, U.S. Geological Survey, Reston, VA.
Sakieh, Y., Salmanmahiny, A., Jafarnezhad, J., Mehri, A., Kamyab, H., Galdavi, S., 2015. Evaluating the strategy of decentralized urban land-use planning in a developing region. Land Use Policy 48, 534–551.
Sang, L.L., Zhang, C., Yang, J.Y., Zhu, D.H., Yun, W.J., 2011. Simulation of land use spatial pattern of towns and villages based on CA– Markov model. Math. Comput. Model. 54, 938–943.
Sangermano, F., Eastman, J. R., Zhu, H., 2010. Similarity Weighted Instance-based Learning for the Generation of Transition Potentials in Land Use Change Modeling. T. GIS. 2010, 14(5), 569–580.
Setyorini, A., Khare, D., Pingale, S.M., 2017. Simulating the impact of land use/land cover change and climate variability on watershed hydrology in the Upper Brantas basin, Indonesia. Appl. Geomat. 9, 191–204.
Shrestha, N.K., Du, X., Wang, J., 2017. Assessing climate change impacts on freshwater resources of the Athsbasca River Basin Canada. Sci. Total Environ. 601, 425–440.
Shrestha, N.K., Wang, J., 2018. Predicting sediment yield and transport dynamics of a cold climate region watershed in changing climate. Sci. Total Environ. 625, 1030–1045.
Stähli, M., Jansson, P.E., Lundin, L.C., 1999. Soil moisture redistribution and infiltration in frozen sandy soils. Water Resour. Res. 35, 95–103.
Sunde, M.G., He, H.S., Hubbart, J.A., Urban, M.A., 2018. An integrated modeling approach for estimating hydrologic responses to future urbanization and climate changes in a mixed use Midwestern watershed. J. Environ. Manage. 220, 149–162.
Swets, J.A., 1986. Measuring the accuracy of diagnostic systems. Science 240, 1285–1293.
Sangermano, F., Eastman, J.R., Zhu, H., 2010b. Similarity weighted instance based learning for the generation of transition potentials in land change modeling. Trans. GIS 14 (5), 569–580.
Tayyebi, A., Delavar, M.R., Yazdanpanah, M.J., Pijanowski, B.C., Saeedi, S., Tayyebi, A.H., 2010. A spatial logistic regression model for simulating land use patterns, a case study of the shiraz metropolitan area of Iran. In: In: Chuvieco, E., Li, J., Yang, X. (Eds.), Advances in earth observation of global change Springer Press.
Teshager, A.D., Gassman, P.W., Schoof, J.T., Secchi, S., 2016. Assessment of impacts of agricultural and climate change scenarios on watershed water quantity and quality, and crop production. Hydrol. Earth Syst. Sci. 20, 3325–3342.
Teutschbein, C., Seibert, J., 2012. Bias correction of regional climate modelsimulations for hydrological climate-change impact studies: review andevaluation of different methods. J. Hydrol. 456–457, 12–29.
Thapa, Rajesh, Murayama, Yuji, 2012. Scenario based urban growth allocation in Kathmandu Valley, Nepal. Landsc. Urban Plann. 105, 140–148. https://doi.org/10.1016/j.landurbplan.2011.12.007.
Trolle, D., Nielsen, A., Rolighed, J., Thodsen, H., Andersen, H.E., Karlsson, I.B., Refsgaard, J.C., Olesen, J.E., Bolding, K., Sondergaard, M., Jeppesen, E., 2015. Projecting the future ecological state of lakes in Denmark in a 6 degree warming scenario. Clim. Res. 64, 55–72.
US Environmental Protection Agency (USEPA), 1997. Climate change and New Jersey. Available at: https://nepis.epa.gov/Exe/ZyNET.exe/40000IXI.txt?ZyActionD=ZyDocument&Client=EPA&Index=1995%20Thru%201999&Docs=&Query=&Time=&EndTime=&SearchMethod=1&TocRestrict=n&Toc=&TocEntry=&QField=&QFieldYear=&QFieldMonth=&QFieldDay=&UseQField=&IntQFieldOp=0&ExtQFieldOp=0&XmlQuery=&File=D%3A%5CZYFILES%5CINDEX%20DATA%5C95THRU99%5CTXT%5C00000010%5C40000IXI.txt&User=ANONYMOUS&Password=anonymous&SortMethod=h%7C-&MaximumDocuments=1&FuzzyDegree=0&ImageQuality=r75g8/r75g8/x150y150g16/i425&Display=hpfr&DefSeekPage=x&SearchBack=ZyActionL&Back=ZyActionS&BackDesc=Results%20page&MaximumPages=1&ZyEntry=2. (accessed 10.6.2018).
US Environmental Protection Agency (USEPA), 2016. What climate change means for New Jersey. EPA 430-F-16-032. Available at: https://19january2017snapshot.epa.gov/sites/production/files/2016-09/documents/climate-change-nj.pdf. (accessed

18.06.2018).
Verburg, P.H., Soepboer, W., Veldkamp, A., Limpiada, R., Espaldon, V., Mastura, S.S.A., 2002. Modeling the spatial dynamics of regional land use: The CLUE-S model. Environ. Manage. 30, 391–405.
Wagena, M.B., Sommerlot, A., Abiy, A.Z., Collick, A.S., Langan, S., Fuka, D.R., Easton, Z.M., 2016. Climate change in the Blue Nile basin Ethiopia: implications for water resources and sediment transport. Clim. Change 139, 229–243.
Wagena, M.B., Easton, Z.M., 2018. Agricultural conservation practices can help mitigate the impact of climate change. Sci. Total Environ. 635, 132–143.
Weber, E.U., 2006. Experience-based and description-based perceptions of long-term risk: why global warming does not scare us (yet). Clim. Change 77, 103–120.
Woznicki, S., Nejadhashemi, A.P., Tang, Y., Wang, L., 2016. Large scale climate change vulnerability assessment of stream health. Ecol. Indic. 69, 578–594.
Wu, F., 2002. Calibration of stochastic cellular automata: the application to rural-urban land conversions. Int. J. Geogr. Inf. Sci. 16, 795–818.
Wu, Y., Liu, S., Abdul-Aziz, O.I., 2012a. a. Hydrological effects of the increased CO2 and climate change in the Upper Mississippi River Basin using a modified SWAT. Clim. Change 110, 977–1003.
Wu, Y., Liu, S., Gallant, A.L., 2012b. b. Predicting impacts of increased CO2 and climate change on the water cycle and water quality in the semiarid James River Basin of the Midwestern USA. Sci. Total Environ. 430, 150–160.
Yan, B., Fang, N.F., Zhang, P.C., Shi, Z.H., 2013. Impacts of land use change on watershed streamflow and sediment yield: an assessment using hydrologic modelling and partial least squares regression. J. Hydrol. 484, 26–37.
Yang, X., Warren, R., He, Y., Ye, J., Li, Q., Wang, G., 2018. Impacts of climate change on Tn load and its control in a river basin with complex pollution sources. Sci. Total Environ. 615, 1155–1163.
Zhang, L., Nan, Z., Yu, W., Zhao, Y., Xu, Y., 2018. Comparison of baseline period choices for separating climate and land use/land cover change impacts on watershed hydrology using distributed hydrological models. Sci. Total Environ. 622–623, 1016–1028.
Zierl, B., Bugmann, H., 2005. Global change impacts on hydrological processes in Alpine catchments. Water Resour. Res. 41, W02028. https://doi.org/10.1029/2004WR003447.